R-708-NYC
JULY 1971

A Water-Quality Simulation Model for Well Mixed Estuaries and Coastal Seas: Vol. II, Computation Procedures

J. J. Leendertse and E. C. Gritton

THE
NEW YORK CITY
RAND
INSTITUTE

545 MADISON AVENUE NEW YORK NEW YORK 10022 (212) 758-2244

Rand

The New York City-Rand Institute is a nonprofit research institution founded, as its Articles of Incorporation state, "... primarily to conduct programs of scientific research and study, and provide reports and recommendations, relevant to the operations, planning or administration of the City of New York." The Institute was established in 1969 by the City of New York and The Rand Corporation as a center for the continuing application of scientific and analytic techniques to problems of urban life and local government. It is governed by a Board of Trustees appointed jointly by the City and Rand.

R-708-NYC
JULY 1971

A Water-Quality Simulation Model for Well Mixed Estuaries and Coastal Seas: Vol. II, Computation Procedures

J. J. Leendertse and E. C. Gritton

This study was sponsored by the City of New York and by the New York City-Rand Institute. Its contents, however, do not purport to represent the official views or policy of the City of New York.

THE
NEW YORK CITY
RAND
INSTITUTE

545 MADISON AVENUE NEW YORK NEW YORK 10022 (212) 758-2244

Rand

Published by The Rand Corporation

PREFACE

This Report is the second volume in a series describing the results of Rand's research in the area of estuarine analysis. In the first volume, *A Water-Quality Simulation Model for Well-Mixed Estuaries and Coastal Seas: Volume I, Principles of Computation* (RM-6230-RC), the basic formulation and principles of computation of the water-quality simulation model were reported. The present study describes the detailed numerical procedures and design philosophy used in the further development of the model, including the addition of a biochemical and biological reaction model. The model is now being evaluated and adjusted in a study of the existing and future water-quality conditions in Jamaica Bay, under contract with the City of New York. The preliminary results of this study obtained from the model are described in a companion Report, *A Water-Quality Simulation Model for Well-Mixed Estuaries and Coastal Seas: Volume III, Jamaica Bay Simulation* (R-709-NYC). The development of this model in its final form will provide a tool for the decisionmaker to analyze various alternatives and their implications associated with the discharge of waste material into coastal waters. This will allow a quantitative assessment of the effects of these discharges on the future water quality of the receiving waters, which may suggest ways of improving water quality.

SUMMARY

This Report describes the progress of a continuing research program related to the development of a water-quality simulation model for well-mixed estuaries and coastal seas, as first outlined in RM-6230-RC. The model developed in RM-6230-RC is extended to include the transport of several waste constituents and a reaction model which simulates the biological and chemical interactions among these constituents in coastal waters. The numerical methods used to approximate the system of partial differential equations describing the tidal flow and dispersion and transport of constituents are described in detail.

The model simulates the changes in boundaries that occur in shallow areas of estuaries as a result of the changing tide level. The procedures used to make these time-dependent boundary changes have been extensively revised from the previous work, and are outlined in this Report.

Examples are given of the necessary input parameters and resultant output data obtained from the computer program developed from this simulation model. The examples are taken from a modeling effort currently under way in Jamaica Bay, Long Island, New York.

CONTENTS

I. INTRODUCTION

It is necessary to quantitatively assess the influence of waste discharges on the water quality of the receiving waters to ensure their proper management. This assessment can be made through the use of simulation models designed to reproduce the water movements and water quality of the area under investigation. After proper verification and adjustment, these models can be used to predict the effect on present water quality of changes in the properties of the waste material discharged in the area or changes in the physical boundaries of the receiving waters.

In a previous Rand Memorandum,[1] a water-quality simulation model was developed for well-mixed estuaries and coastal seas. In the present study, the model has been extended to include the transport of several dissolved waste constituents in the fluid, including any interactions among them. This required the development of a reaction model which simulates the biological and chemical processes, as well as their interactions, in an estuary. The reaction model is completely general, and allows for nonlinear as well as linear interactions among constituents. Thus one is enabled to describe a wide range of biological and biochemical processes. In this Report, the numerical procedures used to solve the equations describing this reaction model and the methods developed to integrate the model into the flow and transport computations are described in detail. In addition, the reader will find a more detailed description of the finite-difference approximations and the numerical procedures used to solve the governing flow and transport equations of the model.

The changing tide level influences the location of the land-water boundaries in the shallow areas of coastal waters. To simulate this process, procedures were developed in the model to allow for time-dependent boundary changes. These procedures are also described, along with the techniques used to suppress the generation and transmission of disturbances due to the discrete changes made in the shape of the boundaries of the tidal flats during the computation.

Large amounts of numerical data are generated by the computer program developed from the simulation model. To assist the investigator in extracting important and meaningful results from these data, machine-made drawings are used to graphically present the results of the computation. Sample outputs from a study of Jamaica Bay, Long Island, New York are used to illustrate these graphical techniques.

II. REACTION MODEL

An important aspect of the development of a water-quality simulation model is the design of a reaction model to describe the biological and chemical processes, as well as their interactions, in an estuary. Because the ecology of an estuary or coastal sea depends on many diverse factors, each of which may at some time become important and warrant study, the reaction model should be as general and flexible as possible. The present study extends the initial work of Leendertse[1] on the transport and dispersion of a single conservative or nonconservative pollutant in a fluid medium to include the transport of several dissolved waste constituents in the fluid, including any interactions among them.

MASS-BALANCE EQUATIONS

The basic mass-balance equation for two-dimensional transport of waste constituents in a well-mixed estuary is given in Ref. 1 as

$$\frac{\partial(HP)}{\partial t} + \frac{\partial(HUP)}{\partial x} + \frac{\partial(HVP)}{\partial y} - \frac{\partial\left(HD_x \frac{\partial P}{\partial x}\right)}{\partial x} - \frac{\partial\left(HD_y \frac{\partial P}{\partial y}\right)}{\partial y} - HS_A = 0 \qquad (1)$$

In the above, P is the integrated average over the vertical of the waste constituent's mass concentration, given by

$$P = \frac{1}{H}\int_{-h}^{\zeta} \rho_A \, dz \qquad (2)$$

where, in Eqs. (1) and (2),

ρ_A = mass density of substance A

ζ = water level elevation relative to the reference plane

h = distance from the reference plane to the bottom

$H = h + \zeta$

S_A = source function

The variables U and V are vertically averaged fluid velocity components, defined as

$$U = \frac{1}{H}\int_{-h}^{\zeta} u \, dz \tag{3}$$

$$V = \frac{1}{H}\int_{-h}^{\zeta} v \, dz \tag{4}$$

where u and v are the fluid speeds along the eastward- and northward-directed axes x and y, respectively. The dispersion coefficients D_x and D_y used in this study are the same as those described in detail in Ref. 1, and therefore will not be treated further here. The source function S_A includes the local addition of substances at any point in the estuary, as well as the rate of production of the substance in the fluid.

Equation (1) describes the transport of a single waste constituent in a fluid. Since the analysis of fluid waste discharges in an estuary can involve the study of several types of substances, this transport equation must be generalized to include the simultaneous transport of several waste constituents. In addition, since the constituents may be transformed during their transport by biochemical, chemical, or physical interactions, one must include a reaction model. The generalized mass-balance equation for n constituents is written in matrix notation as

$$\frac{\partial(H\bar{P})}{\partial t} + \frac{\partial(HU\bar{P})}{\partial x} + \frac{\partial(HV\bar{P})}{\partial y} - \frac{\partial\left(HD_x \frac{\partial \bar{P}}{\partial x}\right)}{\partial x} - \frac{\partial\left(HD_y \frac{\partial \bar{P}}{\partial y}\right)}{\partial y} + [K]H\bar{P} + H\bar{S} = 0 \tag{5}$$

where

$\bar{P}$ = mass-concentration vector containing n constituents

[K] = reaction matrix

$\overline{S}$ = source (or sink) vector

REACTION MATRIX

The reaction matrix [K] in its most general form can give rise to a nonlinear transport equation. This occurs because the individual elements of the matrix can be defined as functions of their own concentration, or that of other constituents, or both. For these reactions, the rate of change of concentration of a particular substance is dependent upon a function of its own concentration or that of other constituents. To illustrate the methods of analysis, only first-order reactions are considered in the present study. Thus, a linear transport equation is obtained, and the first-order reaction matrix considered allows the constituents to decay as well as permitting coupling between individual constituents.

As an example, consider first the modeling of coliform bacteria, which can be assumed to have a first-order reaction decay and to come from three independent groups of sources. For this model, the [K] matrix is a single diagonal matrix and $\overline{P}$ is a column vector containing three elements:

$$[K] = \begin{bmatrix} K_{11} & 0 & 0 \\ 0 & K_{22} & 0 \\ 0 & 0 & K_{33} \end{bmatrix} \quad ; \quad \overline{P} = \begin{bmatrix} P_1 \\ P_2 \\ P_3 \end{bmatrix} \tag{6}$$

where K_{11}, K_{22}, and K_{33} are the first-order decay constants (in most cases $K_{11} = K_{22} = K_{33}$) and P_1, P_2, and P_3 are the concentrations of coliform bacteria from the first, second, and third group of sources, respectively.

The second example studied is the reaction model for the interaction between biochemical oxygen demand (BOD) and dissolved oxygen (DO) in a fluid. The discharge of fluid wastes containing organic matter from such sources as municipal or industrial sewage outfalls has a great effect on the resulting quality of the receiving water. Dissolved oxygen

in the receiving water is used by bacteria in the stabilization of organic matter. The amount of oxygen utilized by the bacteria is measured by the BOD. Replacement of the dissolved oxygen takes place by reaeration at the water surface, and in certain cases by net production throughout the water body by photosynthesis due to the growth of algae. If it is assumed that the BOD resulting from carbonaceous and nitrogenous organic matter can be modeled using a single first-order reaction coefficient, and if photosynthesis is neglected, then the last two terms in Eq. (5) can be written as

$$[K] = \begin{bmatrix} \frac{K_{11}}{H} & K_{12} \\ 0 & K_{22} \end{bmatrix} \quad ; \quad \bar{P} = \begin{bmatrix} P_1 \\ P_2 \end{bmatrix} \tag{7}$$

and

$$\bar{S} = \begin{bmatrix} -\frac{K_{11} C_{SAT}}{H} \\ 0 \end{bmatrix} \tag{8}$$

where

K_{11} = reaeration coefficient of oxygen (ft/sec)

$K_{12} = K_{22}$ = first-order BOD reaction coefficient (sec^{-1})

P_1 = DO concentration (mg/ℓ)

P_2 = BOD concentration (mg/ℓ)

C_{SAT} = saturation concentration of oxygen (mg/ℓ)

Point sources of BOD and DO, such as occur at the location of sewage discharges into the estuary, are simulated by adding delta-function source terms to the source vector. These procedures will be described in more detail in a later section.

In the present model, provision is made for a time-variant, spatially dependent reaeration coefficient. Appropriate values are obtained by matching field measurements taken in the estuary of interest.

The two examples given above are used as a first test for the numerical procedures. The analysis can easily be generalized to include nonlinear reactions by regarding the bacterial decay constants, the reaction coefficients, or the reaeration coefficient as a function of the concentration of the substance itself, of other constituents in the fluid, or of the flow properties of the fluid.

Since the reaction matrix was intentionally designed to be very general, other biological systems can be modeled easily. As an example, one can consider the nonlinear growth and distribution of phytoplankton. These microscopic plants utilize radiant energy from the sun to convert inorganic chemicals present in coastal waters to organic cell material, which in turn is then consumed by animal species in the next higher trophic level (i.e., zooplankton). Depending upon the relative rates of utilization of oxygen by respiration and the production of oxygen by photosynthesis, the presence of phytoplankton can lead to a very important source or sink of oxygen in coastal waters. The set of mass-balance equations describing the interactions among phytoplankton, zooplankton, and nutrients such as nitrogen or phosphorous can be cast into a form similar to those presented for the DO-BOD model. These interactions can then be simulated by using the general reaction model developed in this Report.

In addition to first-order kinetics, the general design of the model permits the reaction rates to be dependent on the age of the constituents. As an example, one can consider the release of bacteria with age-dependent birth and death rates in which the reproductive characteristics change due to selective growth of the more resistant strains. These processes can be included in the model by representing the behavior of a single constituent by several different groups, each with a different decay coefficient. The constituents can then cascade from one group to another as time progresses.

III. FINITE-DIFFERENCE APPROXIMATION TO THE MOMENTUM AND MASS-BALANCE EQUATIONS

The transport of waste constituents throughout an estuary depends upon the flow characteristics of the water-transporting medium. The flow model used in this study is that developed previously by Leendertse.[1] In the flow model, water velocities and water levels are computed throughout the regions of interest. These values are then used in the mass-balance equation to obtain the waste-constituent transport.

For two-dimensional flow in a well-mixed estuary, vertical integration of the momentum and continuity equations yields the following basic equations for the flow model:

$$\frac{\partial U}{\partial t} + U\frac{\partial U}{\partial x} + V\frac{\partial U}{\partial y} - fV + g\frac{\partial \zeta}{\partial x} + g\frac{U(U^2 + V^2)^{\frac{1}{2}}}{C^2 H} - \frac{1}{\rho H}\tau_x^s = 0 \qquad (9)$$

$$\frac{\partial V}{\partial t} + U\frac{\partial V}{\partial x} + V\frac{\partial V}{\partial y} + fU + g\frac{\partial \zeta}{\partial y} + g\frac{V(U^2 + V^2)^{\frac{1}{2}}}{C^2 H} - \frac{1}{\rho H}\tau_y^s = 0 \qquad (10)$$

$$\frac{\partial \zeta}{\partial t} + \frac{\partial (HU)}{\partial x} + \frac{\partial (HV)}{\partial y} = 0 \qquad (11)$$

where

f = Coriolis parameter

g = acceleration of gravity

C = Chezy coefficient

τ_x^s = component of the wind stress in the x direction

τ_y^s = component of the wind stress in the y direction

ρ = water density

The wind-stress components are given by Dronkers[2] as

$$\tau_x^s = \theta \rho_a w^2 \sin \psi$$

and

$$\tau_y^s = \theta \rho_a w^2 \cos \psi$$

where

θ = wind stress coefficient ≈ 0.0026

ρ_a = atmospheric density

w = wind velocity

ψ = angle between the wind direction and the y axis

In the finite-difference approximation of Eqs. (5), (9), (10), and (11), the discrete values of the variables are described on a space-staggered grid as shown in Fig. 1. The water levels ζ and

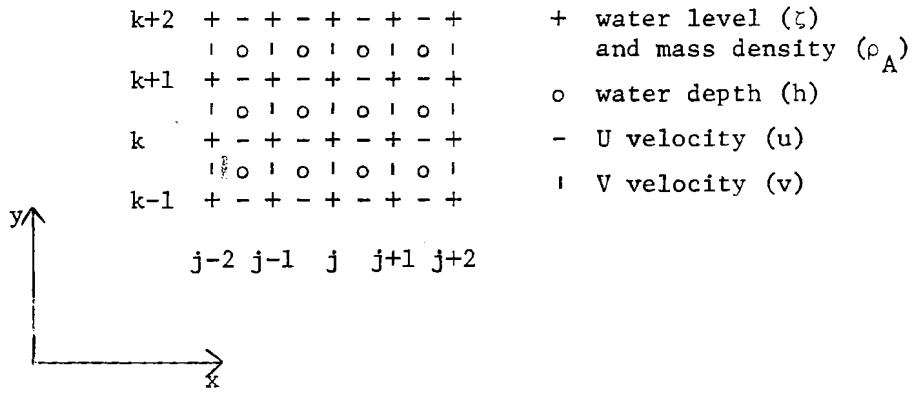

Fig. 1--Space-staggered grid

mass densities ρ_A are computed at integer values of j and k, while the values of h, obtained from a field survey, are given at half-integer values of j and k. The velocities u are computed at half-integer values of j and integer values of k, while the velocities v are computed at half-integer values of k and integer values of j.

Because several of the finite-difference equations in Ref. 1 used to approximate the differential equations contain typographical errors, they are repeated here for completeness. The following notation is used:

$$F \equiv F(j\Delta x, k\Delta y, n\Delta t)$$

where the position and time coordinate (x, y, t) is represented on the finite grid by

$$(j\Delta x,\ k\Delta y,\ n\Delta t) \text{ and } j,\ k,\ n = 0,\ \pm 1/2,\ \pm 1,\ \pm 3/2\ \ldots$$

Averages and differences are symbolically represented by

$$\bar{F}^{x} = \tfrac{1}{2}\{F[(j + \tfrac{1}{2})\Delta x,\ k\Delta y,\ n\Delta t] + F[(j - \tfrac{1}{2})\Delta x,\ k\Delta y,\ n\Delta t]\} \tag{12}$$

$$\delta_{x}F = \frac{1}{\Delta x}\{F[(j + \tfrac{1}{2})\Delta x,\ k\Delta y,\ n\Delta t] - F[(j - \tfrac{1}{2})\Delta x,\ k\Delta y,\ n\Delta t]\} \tag{13}$$

$$\begin{aligned}\bar{\bar{F}} = \tfrac{1}{4}\{&F[(j + \tfrac{1}{2})\Delta x,\ (k + \tfrac{1}{2})\Delta y,\ n\Delta t] + F[(j + \tfrac{1}{2})\Delta x,\ (k - \tfrac{1}{2})\Delta y,\ n\Delta t] \\ &+ F[(j - \tfrac{1}{2})\Delta x,\ (k + \tfrac{1}{2})\Delta y,\ n\Delta t] + F[(j - \tfrac{1}{2})\Delta x,\ (k - \tfrac{1}{2})\Delta y,\ n\Delta t]\}\end{aligned} \tag{14}$$

These are shown only for x, but are also used for y and t. A special notation is used to indicate shifted time levels:

$$\delta_{+\frac{1}{2}t}F = \frac{2}{\Delta t}\{F[j\Delta x,\ k\Delta y,\ (n + \tfrac{1}{2})\Delta t] - F(j\Delta x,\ k\Delta y,\ n\Delta t)\} \tag{15}$$

$$F_{+} = F[j\Delta x,\ k\Delta y,\ (n + \tfrac{1}{2})\Delta t] \tag{16}$$

$$F_{-} = F[j\Delta x,\ k\Delta y,\ (n - \tfrac{1}{2})\Delta t] \tag{17}$$

$$\bar{F}^{t/2} = \tfrac{1}{2}\{F[j\Delta x,\ k\Delta y,\ (n + \tfrac{1}{2})\Delta t] + F[j\Delta x,\ k\Delta y,\ n\Delta t]\} \tag{18}$$

The set of finite-difference equations used to approximate the momentum and mass-balance equations are now presented at two adjacent time levels in the order in which they are computed. For the time level n, we use

Momentum equation

$$\delta_t u - f\bar{\bar{v}} + u_+\overline{\delta_x u_-}^x + \overline{\bar{v}\delta_y u_-}^y + g\overline{\delta_x \zeta}^t$$

$$+ g\frac{\bar{u}^t[(u_-)^2 + (\bar{\bar{v}})^2]^{\frac{1}{2}}}{(\bar{h}^y + \bar{\zeta}^x)(\bar{C}^x)^2} - \frac{1}{\rho(\bar{h}^y + \bar{\zeta}^x)}\tau_x^s = 0$$

$$\text{at } j + \tfrac{1}{2},\ k,\ n \qquad (19)$$

Continuity equation

$$\delta_{+\frac{1}{2}t}\zeta + \delta_x[(\bar{h}^y + \bar{\zeta}^x)u_+] + \delta_y[(\bar{h}^x + \bar{\zeta}^y)v] = 0$$

$$\text{at } j,\ k,\ n \qquad (20)$$

For constituent i, the mass-balance equation is approximated in finite-difference form at time level n by

$$\delta_{+\frac{1}{2}t}[P_i(\bar{\bar{h}} + \zeta)] + \delta_x[(\bar{h}^y + \bar{\zeta}^x)u_+\bar{P}_{i_+}^x] + \delta_y[(\bar{h}^x + \bar{\zeta}^y)v\bar{P}_i^y]$$

$$- \delta_x[(\bar{h}^y + \bar{\zeta}_+^x)D_{x_+}\delta_x P_{i_+}] - \delta_y[(\bar{h}^x + \bar{\zeta}^y)D_y\delta_y P_i]$$

$$+ \sum_{\ell=1}^{i-1}(\bar{\bar{h}} + \zeta_+)K_{i\ell}P_{\ell_+}\alpha_i + \overline{(\bar{\bar{h}} + \zeta)K_{ii}P_i}^{t/2} + \sum_{\ell=i+1}^{\ell_{max}}(\bar{\bar{h}} + \zeta)K_{i\ell}P_\ell\beta_i$$

$$+ (\bar{\bar{h}} + \zeta)S_i = 0 \qquad \text{at } j,\ k,\ n \qquad (21)$$

where

$$\alpha_i = \begin{cases} 0 & i = 1 \\ 1 & 1 < i \le \ell_{max} \end{cases}$$

$$\beta_i = \begin{cases} 0 & i = \ell_{max} \\ 1 & 1 \le i < \ell_{max} \end{cases}$$

ℓ_{max} = maximum number of constituents

The finite-difference approximations at time level $n + \frac{1}{2}$ are

Momentum equation

$$\delta_t v + f\bar{\bar{u}} + \overline{\bar{u}\delta_x v_-}^x + v_+\overline{\delta_y v_-}^y + g\overline{\delta_y \zeta}^t$$

$$+ g\frac{\bar{v}^t[(\bar{\bar{u}})^2 + (v_-)^2]^{\frac{1}{2}}}{(\bar{h}^x + \bar{\zeta}^y)(\bar{C}^y)^2} - \frac{1}{\rho(\bar{h}^x + \bar{\zeta}^y)}\tau_y^s = 0$$

$$\text{at } j,\ k + \tfrac{1}{2},\ n + \tfrac{1}{2} \qquad (22)$$

Continuity equation

$$\delta_{+\frac{1}{2}t}\zeta + \delta_x[(\bar{h}^y + \bar{\zeta}^x)u] + \delta_y[(\bar{h}^x + \bar{\zeta}^y)v_+] = 0$$

$$\text{at } j,\ k,\ n + \tfrac{1}{2} \qquad (23)$$

Mass-balance equation

$$\delta_{+\frac{1}{2}t}[P_i(\bar{\bar{h}} + \zeta)] + \delta_x[(\bar{h}^y + \bar{\zeta}^x)u\bar{P}_i^x] + \delta_y[(\bar{h}^x + \bar{\zeta}^y)v_+\bar{P}_{i_+}^y]$$

$$- \delta_x[(\bar{h}^y + \bar{\zeta}^x)D_x\delta_x P_i] - \delta_y[(\bar{h}^x + \bar{\zeta}_+^y)D_{y_+}\delta_y P_{i_+}]$$

$$+ \sum_{\ell=1}^{i-1}(\bar{\bar{h}} + \zeta)K_{i\ell}P_\ell\alpha_i + \overline{(\bar{\bar{h}} + \zeta)K_{ii}P_i}^{t/2} + \sum_{\ell=i+1}^{\ell_{max}}(\bar{\bar{h}} + \zeta_+)K_{i\ell}P_{\ell_+}\beta_i$$

$$+ (\bar{\bar{h}} + \zeta)S_i = 0 \qquad \text{at } j,\ k,\ n + \tfrac{1}{2} \qquad (24)$$

As indicated in Eqs. (21) and (24), numerical computation of the reaction matrix terms in the mass-balance equations is accomplished by a sequential use of forward and backward information. As an example, if ℓ_{max} constituents are transported in the fluid, we use for constituent i (where $1 \le i \le \ell_{max}$) in the first operation at time level n

(going from t to $t + \frac{1}{2}\Delta t$) information in the reaction matrix terms on the level $t + \frac{1}{2}\Delta t$ for all constituents for which the sequence number ℓ is smaller than i. Information at the level t is used for all constituents which have a sequence number larger than i. In this step, the constituents are computed in ascending order i = 1 to $i = \ell_{max}$.

In the second operation, at time level $n + \frac{1}{2}$ (going from $t + \frac{1}{2}\Delta t$ to $t + \Delta t$), the constituents are computed in descending order $i = \ell_{max}$ to i = 1. Information on the level $t + \frac{1}{2}\Delta t$ is used for all constituents in the reaction matrix terms which have a sequence number smaller than i and information on the level $t + \Delta t$ is used for all constituents having a number larger than i. This procedure centers the reaction matrix information of the mass balance equations within the time interval t to $t + \Delta t$. The reaction matrix terms which involve the i^{th} constituent itself are taken centered over each half timestep.

The sequential use of the finite-difference approximation to the continuity equations (20) and (23) results in the use of the spatial derivatives alternatingly forward and backward. Thus, over a whole time step the use of this procedure results in terms that are either central in time or averaged over that time interval.

The order of the numerical solution of the finite-difference equations is as follows. In the first operation at time level n (going from t to $t + \frac{1}{2}\Delta t$), the momentum and continuity equations, Eqs. (19) and (20), are solved first for the water levels and velocities in the x direction, u, at time level $n + \frac{1}{2}$. This information is then used in the mass balance equation, Eq. (21), to obtain the constituent concentrations, $P_i^{n+\frac{1}{2}}$, at time level $n + \frac{1}{2}$. The results of this first operation are then used at time level $n + \frac{1}{2}$ to determine the unknowns in the second half time step, going from $t + \frac{1}{2}\Delta t$ to $t + \Delta t$. Again, the momentum and continuity equations, Eqs. (22) and (23) are solved first, only this time the water levels and velocities in the y direction, v, at time level n + 1 are obtained. This new information is then used in the mass balance equation, Eq. (24), to obtain the constituent concentrations, P_i^{n+1}, at time level n + 1. This procedure is then repeated for each succeeding full time step.

The numerical solution of the finite-difference equations presented above has shown that the structure used leads to stable solutions in both time and space. Currently, other properties of these approximations, i.e., their conservation properties (energy, mass, circulation, etc.), are being studied in an attempt to develop an improved structure for the finite-difference scheme that more closely approximates important physical properties of the differential equations, while still staying within the framework of the computational method. The modifications would be mainly in the advection terms of the momentum equation. The results of this investigation will be reported separately. As this information becomes available it will be incorporated into the structure of the current computational methods.

IV. NUMERICAL PROCEDURES FOR THE FLOW COMPUTATION

In each of Eqs. (19) and (20) there are three unknown values to be found at the time level $n + \frac{1}{2}$, which are all on a line k. In Eq. (20) the unknowns are $u^{n+\frac{1}{2}}_{j-\frac{1}{2},k}$, $\zeta^{n+\frac{1}{2}}_{j,k}$, $u^{n+\frac{1}{2}}_{j+\frac{1}{2},k}$ and in Eq. (19) they are $\zeta^{n+\frac{1}{2}}_{j,k}$, $u^{n+\frac{1}{2}}_{j+\frac{1}{2},k}$, and $\zeta^{n+\frac{1}{2}}_{j+1,k}$. Thus in each equation three adjacent values of u and ζ are involved in the computation. This leads to a matrix representation of the finite-difference equations:

$$[A]\{F\} = \{B\}$$

The vector F contains all of the unknown values of u and ζ at time level $n + \frac{1}{2}$, while the vector B contains all of the known information computed from time levels n and $n - \frac{1}{2}$. The matrix [A] is a tridiagonal matrix containing the coefficients of the unknown values of u and ζ. The solution of this matrix equation is carried out in the following sections.

EXPANSION OF THE FINITE-DIFFERENCE EQUATIONS

Expanding the continuity equation given by Eq. (20) for time level n yields

$$\frac{2}{\Delta t}\left(\zeta^{n+\frac{1}{2}}_{j,k} - \zeta^{n}_{j,k}\right) + \left[\left(h_{j+\frac{1}{2},k+\frac{1}{2}} + h_{j+\frac{1}{2},k-\frac{1}{2}} + \zeta^{n}_{j+1,k} + \zeta^{n}_{j,k}\right)u^{n+\frac{1}{2}}_{j+\frac{1}{2},k}\right.$$

$$\left. - \left(h_{j-\frac{1}{2},k+\frac{1}{2}} + h_{j-\frac{1}{2},k-\frac{1}{2}} + \zeta^{n}_{j-1,k} + \zeta^{n}_{j,k}\right)u^{n+\frac{1}{2}}_{j-\frac{1}{2},k}\right]\frac{1}{2\Delta x}$$

$$+ \left[\left(h_{j+\frac{1}{2},k+\frac{1}{2}} + h_{j-\frac{1}{2},k+\frac{1}{2}} + \zeta^{n}_{j,k+1} + \zeta^{n}_{j,k}\right)v^{n}_{j,k+\frac{1}{2}}\right.$$

$$\left. - \left(h_{j+\frac{1}{2},k-\frac{1}{2}} + h_{j-\frac{1}{2},k-\frac{1}{2}} + \zeta^{n}_{j,k} + \zeta^{n}_{j,k-1}\right)v^{n}_{j,k-\frac{1}{2}}\right]\frac{1}{2\Delta x} = 0 \qquad (25)$$

which can be rewritten as

$$-r_{j-\frac{1}{2}}u^{n+\frac{1}{2}}_{j-\frac{1}{2},k} + \zeta^{n+\frac{1}{2}}_{j,k} + r_{j+\frac{1}{2}}u^{n+\frac{1}{2}}_{j+\frac{1}{2},k} = A^{n}_{j} \qquad (26)$$

where the following variables are used:

$$r_{j-\frac{1}{2}} = (h_{j-\frac{1}{2},k+\frac{1}{2}} + h_{j-\frac{1}{2},k-\frac{1}{2}} + \zeta^n_{j-1,k} + \zeta^n_{j,k}) \frac{\Delta t}{4\Delta x} \tag{27}$$

$$r_{j+\frac{1}{2}} = (h_{j+\frac{1}{2},k+\frac{1}{2}} + h_{j+\frac{1}{2},k-\frac{1}{2}} + \zeta^n_{j+1,k} + \zeta^n_{j,k}) \frac{\Delta t}{4\Delta x} \tag{28}$$

$$A^n_j = \zeta^n_{j,k} + (h_{j+\frac{1}{2},k-\frac{1}{2}} + h_{j-\frac{1}{2},k-\frac{1}{2}} + \zeta^n_{j,k} + \zeta^n_{j,k-1}) v^n_{j,k-\frac{1}{2}} \left(\frac{\Delta t}{4\Delta x}\right)$$

$$- (h_{j+\frac{1}{2},k+\frac{1}{2}} + h_{j-\frac{1}{2},k+\frac{1}{2}} + \zeta^n_{j,k+1} + \zeta^n_{j,k}) v^n_{j,k+\frac{1}{2}} \left(\frac{\Delta t}{4\Delta x}\right) \tag{29}$$

The expansion of Eq. (19), the momentum equation, yields:

$$\frac{1}{\Delta t}\left(u^{n+\frac{1}{2}}_{j+\frac{1}{2},k} - u^{n-\frac{1}{2}}_{j+\frac{1}{2},k}\right) - f\bar{\bar{v}} + \left(u^{n-\frac{1}{2}}_{j+\frac{3}{2},k} - u^{n-\frac{1}{2}}_{j-\frac{1}{2},k}\right) u^{n+\frac{1}{2}}_{j+\frac{1}{2},k} \frac{1}{2\Delta x}$$

$$+ \left(u^{n-\frac{1}{2}}_{j+\frac{1}{2},k+1} - u^{n-\frac{1}{2}}_{j+\frac{1}{2},k-1}\right) \frac{\bar{\bar{v}}}{2\Delta x} + \left(\zeta^{n+\frac{1}{2}}_{j+1,k} - \zeta^{n+\frac{1}{2}}_{j,k} + \zeta^{n-\frac{1}{2}}_{j+1,k} - \zeta^{n-\frac{1}{2}}_{j,k}\right) \frac{g}{2\Delta x}$$

$$+ \frac{\left(\frac{g}{2}\right)\left(u^{n+\frac{1}{2}}_{j+\frac{1}{2},k} + u^{n-\frac{1}{2}}_{j+\frac{1}{2},k}\right)\left[\left(u^{n-\frac{1}{2}}_{j+\frac{1}{2},k}\right)^2 + (\bar{\bar{v}})^2\right]^{\frac{1}{2}}}{(\bar{h}^y + \bar{\zeta}^x)(\bar{C}^x)^2} - \frac{1}{\rho(\bar{h}^y + \bar{\zeta}^x)} \tau^s_x = 0$$

$$\text{at } j + \tfrac{1}{2},\ k,\ n \tag{30}$$

where

$$\bar{\bar{v}} = \tfrac{1}{4}(v^n_{j+1,k+\frac{1}{2}} + v^n_{j,k+\frac{1}{2}} + v^n_{j,k-\frac{1}{2}} + v^n_{j+1,k-\frac{1}{2}})$$

$$\bar{h}^y = \tfrac{1}{2}(h_{j+\frac{1}{2},k+\frac{1}{2}} + h_{j+\frac{1}{2},k-\frac{1}{2}})$$

$$\bar{\zeta}^x = \tfrac{1}{2}(\zeta^n_{j+1,k} + \zeta^n_{j,k})$$

$$\bar{C}^x = \tfrac{1}{2}(C^n_{j+1,k} + C^n_{j,k})$$

This expansion can be written in a more compact form as

$$-r_j \zeta^{n+\frac{1}{2}}_{j,k} + r'_{j+\frac{1}{2}} u^{n+\frac{1}{2}}_{j+\frac{1}{2},k} + r_{j+1} \zeta^{n+\frac{1}{2}}_{j+1,k} = B^n_{j+\frac{1}{2},k} \tag{31}$$

where

$$r_j = r_{j+1} = \frac{g\Delta t}{2\Delta x} \tag{32}$$

$$r'_{j+\frac{1}{2}} = 1 + \frac{\Delta t}{2\Delta x}\left(u^{n-\frac{1}{2}}_{j+\frac{3}{2},k} - u^{n-\frac{1}{2}}_{j-\frac{1}{2},k}\right) + \frac{\frac{g\Delta t}{2}\left[\left(u^{n-\frac{1}{2}}_{j+\frac{1}{2},k}\right)^2 + (\bar{\bar{v}})^2\right]^{\frac{1}{2}}}{(\bar{h}^y + \bar{\zeta}^x)(\bar{C}^x)^2} \tag{33}$$

$$B^n_{j+\frac{1}{2},k} = u^{n-\frac{1}{2}}_{j+\frac{1}{2},k} + \left[f\Delta t - \frac{\Delta t}{2\Delta x}\left(u^{n-\frac{1}{2}}_{j+\frac{1}{2},k+1} - u^{n-\frac{1}{2}}_{j+\frac{1}{2},k-1}\right)\right]\bar{\bar{v}}$$

$$- g\frac{\Delta t}{2\Delta x}\left(\zeta^{n-\frac{1}{2}}_{j+1,k} - \zeta^{n-\frac{1}{2}}_{j,k}\right) - \frac{\frac{g\Delta t}{2} u^{n-\frac{1}{2}}_{j+\frac{1}{2},k}\left[\left(u^{n-\frac{1}{2}}_{j+\frac{1}{2},k}\right)^2 + (\bar{\bar{v}})^2\right]^{\frac{1}{2}}}{(\bar{h}^y + \bar{\zeta}^x)(\bar{C}^x)^2}$$

$$+ \frac{1}{\rho(\bar{h}^y + \bar{\zeta}^x)} \tau^s_x \tag{34}$$

RECURSION FORMULAS

Equations (26) and (31) can be solved for the unknown values of velocities and water levels on each row k once boundary conditions are specified at either end of the row. The boundary conditions can be specified so that there are open or closed boundaries at either the right or left side of the computational field, and given values of velocities or water levels can be used as input conditions. To illustrate the method, an open boundary is assumed along part of the left-hand side of the field, while the right-hand side is assumed to be completely closed. Thus, assuming that $\zeta^{n+\frac{1}{2}}_{1,k}$ is a given input level along the left-hand boundary (which can be time varying to simulate tidal motion) and that $u^{n+\frac{1}{2}}_{I+\frac{1}{2}}$ is a known velocity at the right-hand boundary (taken to be zero in this example), then Eqs. (26) and (31) can be written in the matrix form

$$\begin{bmatrix} r'_{J+\frac{1}{2}} & r_{J+1} & 0 & 0 & 0 & \cdots & 0 \\ -r_{J+\frac{1}{2}} & 1 & r_{J+\frac{3}{2}} & 0 & 0 & \cdots & 0 \\ 0 & -r_{J+1} & r'_{J+\frac{3}{2}} & r_{J+2} & 0 & \cdots & 0 \\ 0 & 0 & -r_{J+\frac{3}{2}} & 1 & r_{J+\frac{5}{2}} & \cdots & 0 \\ \vdots & \vdots & \vdots & \vdots & \vdots & \vdots & \vdots \\ \vdots & \vdots & \vdots & \vdots & \vdots & \vdots & \vdots \\ 0 & 0 & \cdots & \cdots & \cdots & -r_{I-\frac{1}{2}} & 1 \end{bmatrix} \begin{bmatrix} u_{J+\frac{1}{2}} \\ \zeta_{J+1} \\ u_{J+\frac{3}{2}} \\ \zeta_{J+2} \\ u_{J+\frac{5}{2}} \\ \vdots \\ u_{I-\frac{1}{2}} \\ \zeta_I \end{bmatrix}^{n+\frac{1}{2}} = \begin{bmatrix} B_{J+\frac{1}{2}} \\ A_{J+1} \\ B_{J+\frac{3}{2}} \\ A_{J+2} \\ \vdots \\ \vdots \\ A_I \end{bmatrix}^{n} + \begin{bmatrix} r_J \zeta_J \\ 0 \\ 0 \\ 0 \\ \vdots \\ \vdots \\ -r_{I+\frac{1}{2}} u_{I+\frac{1}{2}} \end{bmatrix}^{n+\frac{1}{2}} \tag{35}$$

where J = 1, the left-hand boundary, and j = I, the right-hand boundary.

The unknown velocities and water levels in the vector ($u_{J+\frac{1}{2}}$, ζ_{J+1}, $u_{J+\frac{3}{2}}$, ..., ζ_I) at the time level ($n + \frac{1}{2}$) can be easily computed from a series of recursion formulas. Starting with the first equation of the matrix, we find that the velocity $u^{n+\frac{1}{2}}_{J+\frac{1}{2}}$ is expressed as a function of the unknown water level $\zeta^{n+\frac{1}{2}}_{J+1}$ by

$$u^{n+\frac{1}{2}}_{J+\frac{1}{2}} = -R_J \zeta^{n+\frac{1}{2}}_{J+1} + S_J \tag{36}$$

where

$$R_J = \frac{r_{J+1}}{r'_{J+\frac{1}{2}}} \tag{37}$$

$$S_J = \frac{B^n_{J+\frac{1}{2}} + r_J \zeta^{n+\frac{1}{2}}_J}{r'_{J+\frac{1}{2}}} \tag{38}$$

Writing out the second equation of the matrix and using Eq. (36) for $u^{n+\frac{1}{2}}_{J+\frac{1}{2}}$ leads to

$$-r_{J+\frac{1}{2}}\left[-R_J \zeta^{n+\frac{1}{2}}_{J+1} + S_J\right] + \zeta^{n+\frac{1}{2}}_{J+1} + r_{J+\frac{3}{2}} u^{n+\frac{1}{2}}_{J+\frac{3}{2}} = A^n_{J+1}$$

or writing $\zeta^{n+\frac{1}{2}}_{J+1}$ in terms of $u^{n+\frac{1}{2}}_{J+\frac{3}{2}}$ yields

$$\zeta_{J+1}^{n+\frac{1}{2}} = -P_{J+1} u_{J+\frac{3}{2}}^{n+\frac{1}{2}} + Q_{J+1} \tag{39}$$

where

$$P_{J+1} = \frac{r_{J+\frac{3}{2}}}{1 + r_{J+\frac{1}{2}} R_J} \tag{40}$$

$$Q_{J+1} = \frac{A_{J+1}^n + r_{J+\frac{1}{2}} S_J}{1 + r_{J+\frac{1}{2}} R_J} \tag{41}$$

In the same manner, the next velocity can be expressed as a function of the following water level using the third equation of the matrix:

$$u_{J+\frac{3}{2}}^{n+\frac{1}{2}} = -R_{J+1} \zeta_{J+2}^{n+\frac{1}{2}} + S_{J+1} \tag{42}$$

where

$$R_{J+1} = \frac{r_{J+2}}{r'_{J+\frac{3}{2}} + r_{J+1} P_{J+1}} \tag{43}$$

$$S_{J+1} = \frac{B_{J+\frac{3}{2}}^n + r_{J+1} Q_{J+1}}{r'_{J+\frac{3}{2}} + r_{J+1} P_{J+1}} \tag{44}$$

Thus the following general recursion relationships for the unknown velocities and water levels can be written

$$\zeta_j^{n+\frac{1}{2}} = -P_j u_{j+\frac{1}{2}}^{n+\frac{1}{2}} + Q_j \tag{45}$$

$$u_{j-\frac{1}{2}}^{n+\frac{1}{2}} = -R_{j-1} \zeta_j^{n+\frac{1}{2}} + S_{j-1} \tag{46}$$

where

$$P_j = \frac{r_{j+\frac{1}{2}}}{1 + r_{j-\frac{1}{2}} R_{j-1}} \tag{47}$$

$$Q_j = \frac{A_j^n + r_{j-\frac{1}{2}} S_{j-1}}{1 + r_{j-\frac{1}{2}} R_{j-1}} \tag{48}$$

$$R_j = \frac{r_{j+1}}{r'_{j+\frac{1}{2}} + r_j P_j} \tag{49}$$

$$S_j = \frac{B_{j+\frac{1}{2}}^n + r_j Q_j}{r'_{j+\frac{1}{2}} + r_j P_j} \tag{50}$$

The recursion factors R, S, P, and Q are calculated in succession starting with j = 1, the left-hand boundary. Since an open boundary has been assumed over part of the left-hand side of the field, Eqs. (37) and (38) are used first, and initially knowing $\zeta_1^{n+\frac{1}{2}}$, R_1 and S_1 can be calculated. Equations (47) to (50 are then used to calculate the remaining recursion factors. Because the velocity $u_{I+\frac{1}{2}}^{n+\frac{1}{2}}$ is a given boundary condition at the right-hand side of the field, P_I and Q_I are the last recursion factors computed. The water level $\zeta_I^{n+\frac{1}{2}}$ is then found from Eq. (45), and all velocities and water levels are then computed in descending order using Eqs. (45) and (46) recursively.

The computation of the velocities $v_{k+\frac{1}{2}}^{n+1}$ and water levels ζ_k^{n+1} during the second operation, going from time level $n + \frac{1}{2}$ to $n + 1$, is carried out in the same manner as described for Eqs. (19) and (20). Equations (22) and (23) are expanded and put into matrix form. From this matrix equation, recursion relationships similar in form to Eqs. (45) to (50) are developed. Again, both closed or open boundaries are possible at either the top or bottom of the grid.

Local discharges of fresh water from sewage or storm water outfalls are accounted for in the model by increasing the local water level in the continuity equation by an appropriate amount at the discrete points where the outfalls are located. For a discharge rate of 100 ft^3/sec, a grid size of 500 ft, and a half timestep of 50 seconds, this amounts to a water level increase of approximately .02 ft over the area of one grid. This is found not to affect the stability of the computation near these outfalls.

V. NUMERICAL PROCEDURES FOR THE MASS TRANSPORT AND REACTION MODEL

The solution of Eqs. (19) and (20) yields the x component of the water velocity and the water levels at the time level $n + \frac{1}{2}$. These values, along with the y component of the water velocity at time level n, are then used in Eq. (21) to solve for the constituent concentration at time level $n + \frac{1}{2}$. For each constituent i, three unknown values are found at adjacent grid points in Eq. (21), and numerical procedures similar to those in the flow computation can be used to solve for these unknowns. This procedure is described in detail below.

EXPANSION OF THE FINITE-DIFFERENCE EQUATION

In the first operation at time level n (going from t to $t + \frac{1}{2}\Delta t$), the constituents are computed in ascending order $i = 1$ to $i = \ell_{max}$. Thus for constituent i the concentration of all constituents with an index ℓ less than i has already been computed for time level $n + \frac{1}{2}$, and this information is used in the computation of the concentration of the i^{th} constituent. The finite-difference equation for constituent i, Eq. (21), can then be expanded in the form

$$
\begin{aligned}
&[P^{n+\frac{1}{2}}_{j,k;i}(h_{j-\frac{1}{2},k-\frac{1}{2}} + h_{j-\frac{1}{2},k+\frac{1}{2}} + h_{j+\frac{1}{2},k-\frac{1}{2}} + h_{j+\frac{1}{2},k+\frac{1}{2}} + 4\zeta^{n+\frac{1}{2}}_{j,k}) \\
&- P^{n}_{j,k;i}(h_{j-\frac{1}{2},k-\frac{1}{2}} + h_{j-\frac{1}{2},k+\frac{1}{2}} + h_{j+\frac{1}{2},k-\frac{1}{2}} + h_{j+\frac{1}{2},k+\frac{1}{2}} + 4\zeta^{n}_{j,k})]\,\frac{1}{2\Delta t} \\
&- [(\zeta^{n}_{j-1,k} + \zeta^{n}_{j,k} + h_{j-\frac{1}{2},k-\frac{1}{2}} + h_{j-\frac{1}{2},k+\frac{1}{2}})u^{n+\frac{1}{2}}_{j-\frac{1}{2},k}(P^{n+\frac{1}{2}}_{j-1,k;i} + P^{n+\frac{1}{2}}_{j,k;i}) \\
&- (\zeta^{n}_{j,k} + \zeta^{n}_{j+1,k} + h_{j+\frac{1}{2},k-\frac{1}{2}} + h_{j+\frac{1}{2},k+\frac{1}{2}})u^{n+\frac{1}{2}}_{j+\frac{1}{2},k}(P^{n+\frac{1}{2}}_{j,k;i} + P^{n+\frac{1}{2}}_{j+1,k;i})]\left(\frac{1}{4\Delta x}\right) \\
&- [(\zeta^{n}_{j,k-1} + \zeta^{n}_{j,k} + h_{j-\frac{1}{2},k-\frac{1}{2}} + h_{j+\frac{1}{2},k-\frac{1}{2}})v^{n}_{j,k-\frac{1}{2}}(P^{n}_{j,k-1;i} + P^{n}_{j,k;i}) \\
&- (\zeta^{n}_{j,k} + \zeta^{n}_{j,k+1} + h_{j-\frac{1}{2},k+\frac{1}{2}} + h_{j+\frac{1}{2},k+\frac{1}{2}})v^{n}_{j,k+\frac{1}{2}}(P^{n}_{j,k+1;i} + P^{n}_{j,k;i})]\left(\frac{1}{4\Delta x}\right) \\
&+ [(\zeta^{n+\frac{1}{2}}_{j-1,k} + \zeta^{n+\frac{1}{2}}_{j,k} + h_{j-\frac{1}{2},k-\frac{1}{2}} + h_{j-\frac{1}{2},k+\frac{1}{2}})D^{n+\frac{1}{2}}_{x_{j-\frac{1}{2},k}}(P^{n+\frac{1}{2}}_{j,k;i} - P^{n+\frac{1}{2}}_{j-1,k;i}) \\
&- (\zeta^{n+\frac{1}{2}}_{j,k} + \zeta^{n+\frac{1}{2}}_{j+1,k} + h_{j+\frac{1}{2},k-\frac{1}{2}} + h_{j+\frac{1}{2},k+\frac{1}{2}})D^{n+\frac{1}{2}}_{x_{j+\frac{1}{2},k}}(P^{n+\frac{1}{2}}_{j+1,k;i} - P^{n+\frac{1}{2}}_{j,k;i})]\left[\frac{1}{2(\Delta x)^2}\right]
\end{aligned}
$$

$$+ [(\zeta^n_{j,k-1} + \zeta^n_{j,k} + h_{j-\frac{1}{2},k-\frac{1}{2}} + h_{j+\frac{1}{2},k-\frac{1}{2}})D^n_{y_{j,k-\frac{1}{2}}}(P^n_{j,k;i} - P^n_{j,k-1;i})$$

$$- (\zeta^n_{j,k} + \zeta^n_{j,k+1} + h_{j-\frac{1}{2},k+\frac{1}{2}} + h_{j+\frac{1}{2},k+\frac{1}{2}})D^n_{y_{j,k+\frac{1}{2}}}(P^n_{j,k+1;i} - P^n_{j,k;i})]\left[\frac{1}{2(\Delta x)^2}\right]$$

$$+ \sum_{\ell=1}^{i-1} (h_{j+\frac{1}{2},k+\frac{1}{2}} + h_{j+\frac{1}{2},k-\frac{1}{2}} + h_{j-\frac{1}{2},k+\frac{1}{2}} + h_{j-\frac{1}{2},k-\frac{1}{2}} + 4\zeta^{n+\frac{1}{2}}_{j,k})\frac{K_{i\ell}P^{n+\frac{1}{2}}_{j,k;\ell}}{4}\alpha_i$$

$$+ [(h_{j+\frac{1}{2},k+\frac{1}{2}} + h_{j+\frac{1}{2},k-\frac{1}{2}} + h_{j-\frac{1}{2},k+\frac{1}{2}} + h_{j-\frac{1}{2},k-\frac{1}{2}} + 4\zeta^{n+\frac{1}{2}}_{j,k})K_{ii}P^{n+\frac{1}{2}}_{j,k;i}$$

$$+ (h_{j+\frac{1}{2},k+\frac{1}{2}} + h_{j+\frac{1}{2},k-\frac{1}{2}} + h_{j-\frac{1}{2},k+\frac{1}{2}} + h_{j-\frac{1}{2},k-\frac{1}{2}} + 4\zeta^n_{j,k})K_{ii}P^n_{j,k;i}]\left(\frac{1}{8}\right)$$

$$+ \sum_{\ell=i+1}^{\ell_{max}} (h_{j+\frac{1}{2},k+\frac{1}{2}} + h_{j+\frac{1}{2},k-\frac{1}{2}} + h_{j-\frac{1}{2},k+\frac{1}{2}} + h_{j-\frac{1}{2},k-\frac{1}{2}} + 4\zeta^n_{j,k})\frac{K_{i\ell}P^n_{j,k;\ell}}{4}\beta_i$$

$$+ (h_{j+\frac{1}{2},k+\frac{1}{2}} + h_{j+\frac{1}{2},k-\frac{1}{2}} + h_{j-\frac{1}{2},k+\frac{1}{2}} + h_{j-\frac{1}{2},k-\frac{1}{2}} + 4\zeta^n_{j,k})\frac{S^n_{j,k;i}}{4} = 0 \qquad (51)$$

where $P^{n+\frac{1}{2}}_{j,k;i}$ is the concentration of constituent i at the grid point j,k at time level n + ½. The dispersion coefficients D_x, D_y and the source of constituents S_i can be both space- and time-varying functions in this formulation. Point sources of constituents, such as occur at sewage and flood-control outfalls, can be included. The procedures used for this part of the computation are described in Ref. 1.

There are only three unknown variables in Eq. (51). They are

$$P^{n+\frac{1}{2}}_{j,k;i}; \quad P^{n+\frac{1}{2}}_{j-1,k;i} \quad \text{and} \quad P^{n+\frac{1}{2}}_{j+1,k;i}$$

Thus, rewriting Eq. (51) after multiplying through by $\tau = \Delta t/2$ yields

$$a_j P^{n+\frac{1}{2}}_{j-1,k;i} + b_j P^{n+\frac{1}{2}}_{j,k;i} + c_j P^{n+\frac{1}{2}}_{j+1,k;i} = D_j \qquad (52)$$

where:

$$a_j = -(\zeta^n_{j-1,k} + \zeta^n_{j,k} + h_{j-\frac{1}{2},k-\frac{1}{2}} + h_{j-\frac{1}{2},k+\frac{1}{2}})u^{n+\frac{1}{2}}_{j-\frac{1}{2},k}\left(\frac{\tau}{4\Delta x}\right)$$

$$- (\zeta^{n+\frac{1}{2}}_{j-1,k} + \zeta^{n+\frac{1}{2}}_{j,k} + h_{j-\frac{1}{2},k-\frac{1}{2}} + h_{j-\frac{1}{2},k+\frac{1}{2}})D^{n+\frac{1}{2}}_{x_{j-\frac{1}{2},k}}\left[\frac{\tau}{2(\Delta x)^2}\right] \qquad (53)$$

$$c_j = -\left[(\zeta^n_{j,k} + \zeta^n_{j+1,k} + h_{j+\frac{1}{2},k-\frac{1}{2}} + h_{j+\frac{1}{2},k+\frac{1}{2}})(-u^{n+\frac{1}{2}}_{j+\frac{1}{2},k})\right.$$

$$\left. + (\zeta^{n+\frac{1}{2}}_{j,k} + \zeta^{n+\frac{1}{2}}_{j+1,k} + h_{j+\frac{1}{2},k-\frac{1}{2}} + h_{j+\frac{1}{2},k+\frac{1}{2}})D^{n+\frac{1}{2}}_{x_{j+\frac{1}{2},k}}\left(\frac{2}{\Delta x}\right)\right]\left(\frac{\tau}{4\Delta x}\right) \qquad (54)$$

$$b_j = \frac{1}{4}(h_{j-\frac{1}{2},k-\frac{1}{2}} + h_{j-\frac{1}{2},k+\frac{1}{2}} + h_{j+\frac{1}{2},k-\frac{1}{2}} + h_{j+\frac{1}{2},k+\frac{1}{2}}) + \zeta^{n+\frac{1}{2}}_{j,k}$$

$$- (\zeta^n_{j-1,k} + \zeta^n_{j,k} + h_{j-\frac{1}{2},k-\frac{1}{2}} + h_{j-\frac{1}{2},k+\frac{1}{2}})u^{n+\frac{1}{2}}_{j-\frac{1}{2},k}\left(\frac{\tau}{4\Delta x}\right)$$

$$+ (\zeta^n_{j,k} + \zeta^n_{j+1,k} + h_{j+\frac{1}{2},k-\frac{1}{2}} + h_{j+\frac{1}{2},k+\frac{1}{2}})u^{n+\frac{1}{2}}_{j+\frac{1}{2},k}\left(\frac{\tau}{4\Delta x}\right)$$

$$+ (\zeta^{n+\frac{1}{2}}_{j-1,k} + \zeta^{n+\frac{1}{2}}_{j,k} + h_{j-\frac{1}{2},k-\frac{1}{2}} + h_{j-\frac{1}{2},k+\frac{1}{2}})D^{n+\frac{1}{2}}_{x_{j-\frac{1}{2},k}}\left[\frac{\tau}{2(\Delta x)^2}\right]$$

$$+ (\zeta^{n+\frac{1}{2}}_{j,k} + \zeta^{n+\frac{1}{2}}_{j+1,k} + h_{j+\frac{1}{2},k-\frac{1}{2}} + h_{j+\frac{1}{2},k+\frac{1}{2}})D^{n+\frac{1}{2}}_{x_{j+\frac{1}{2},k}}\left[\frac{\tau}{2(\Delta x)^2}\right]$$

$$+ \left[\frac{1}{4}(h_{j+\frac{1}{2},k+\frac{1}{2}} + h_{j+\frac{1}{2},k-\frac{1}{2}} + h_{j-\frac{1}{2},k+\frac{1}{2}} + h_{j-\frac{1}{2},k-\frac{1}{2}}) + \zeta^{n+\frac{1}{2}}_{j,k}\right]\left(\frac{K_{ii}\tau}{2}\right) \qquad (55)$$

$$D_j = P^n_{j,k;i}\left[\frac{1}{4}\left(h_{j-\frac{1}{2},k-\frac{1}{2}} + h_{j-\frac{1}{2},k+\frac{1}{2}} + h_{j+\frac{1}{2},k-\frac{1}{2}} + h_{j+\frac{1}{2},k+\frac{1}{2}}\right) + \zeta^n_{j,k}\right]$$

$$+ \left[\left(\zeta^n_{j,k-1} + \zeta^n_{j,k} + h_{j-\frac{1}{2},k-\frac{1}{2}} + h_{j+\frac{1}{2},k-\frac{1}{2}}\right)v^n_{j,k-\frac{1}{2}}\left(P^n_{j,k-1;i} + P^n_{j,k;i}\right)\right.$$

$$\left. - \left(\zeta^n_{j,k} + \zeta^n_{j,k+1} + h_{j-\frac{1}{2},k+\frac{1}{2}} + h_{j+\frac{1}{2},k+\frac{1}{2}}\right)v^n_{j,k+\frac{1}{2}}\left(P^n_{j,k+1} + P^n_{j,k}\right)\right]\left(\frac{\tau}{4\Delta x}\right)$$

$$- \left[\left(\zeta^n_{j,k-1} + \zeta^n_{j,k} + h_{j-\frac{1}{2},k-\frac{1}{2}} + h_{j+\frac{1}{2},k-\frac{1}{2}}\right)D^n_{y_{j,k-\frac{1}{2}}}\left(P^n_{j,k;i} - P^n_{j,k-1;i}\right)\right.$$

$$\left. - \left(\zeta^n_{j,k} + \zeta^n_{j,k+1} + h_{j-\frac{1}{2},k+\frac{1}{2}} + h_{j+\frac{1}{2},k+\frac{1}{2}}\right)D^n_{y_{j,k+\frac{1}{2}}}\left(P^n_{j,k+1;i} - P^n_{j,k;i}\right)\right]\left[\frac{\tau}{2(\Delta x)^2}\right]$$

$$- \sum_{\ell=1}^{i-1}\left[\frac{1}{4}\left(h_{j+\frac{1}{2},k+\frac{1}{2}} + h_{j+\frac{1}{2},k-\frac{1}{2}} + h_{j-\frac{1}{2},k+\frac{1}{2}} + h_{j-\frac{1}{2},k-\frac{1}{2}}\right) + \zeta^{n+\frac{1}{2}}_{j,k}\right]K_{i\ell}\tau P^{n+\frac{1}{2}}_{j,k;\ell}\alpha_i$$

$$- \left[\frac{1}{4}\left(h_{j+\frac{1}{2},k+\frac{1}{2}} + h_{j+\frac{1}{2},k-\frac{1}{2}} + h_{j-\frac{1}{2},k+\frac{1}{2}} + h_{j-\frac{1}{2},k-\frac{1}{2}}\right) + \zeta^n_{j,k}\right]\frac{K_{ii}\tau P^n_{j,k;i}}{2}$$

$$- \sum_{\ell=i+1}^{\ell_{max}}\left[\frac{1}{4}\left(h_{j+\frac{1}{2},k+\frac{1}{2}} + h_{j+\frac{1}{2},k-\frac{1}{2}} + h_{j-\frac{1}{2},k+\frac{1}{2}} + h_{j-\frac{1}{2},k-\frac{1}{2}}\right) + \zeta^n_{j,k}\right]K_{i\ell}\tau P^n_{j,k;\ell}\beta_i$$

$$- \left[\frac{1}{4}\left(h_{j+\frac{1}{2},k+\frac{1}{2}} + h_{j+\frac{1}{2},k-\frac{1}{2}} + h_{j-\frac{1}{2},k+\frac{1}{2}} + h_{j-\frac{1}{2},k-\frac{1}{2}}\right) + \zeta^n_{j,k}\right]S^n_{j,k;i}\tau \tag{56}$$

For each row k and constituent i, Eq. (52) can be written as

$$a_j P_{j-1} + b_j P_j + c_j P_{j+1} = D_j \tag{57}$$

where the subscripts k;i and superscript $n + \frac{1}{2}$ are dropped for convenience. Equation (57) can be solved for the concentration of constituent i at each grid point along row k by a process of elimination

of unknowns. To illustrate the method, a closed left-hand boundary is assumed at some value of j = J - 1, k = K, as shown in Fig. 2.

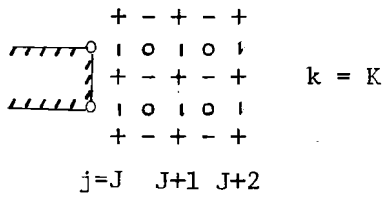

Fig. 2--Left closed boundary

For this case, both the advective and dispersive transport of constituent i through the cross section between grid points J - 1 and J is zero. Thus $a_j \equiv 0$, and Eq. (57) can be written

$$b_J P_J + c_J P_{J+1} = D_J \tag{58}$$

For the next point, j = J + 1, along row k = K, Eq. (57) is written as

$$a_{J+1} P_J + b_{J+1} P_{J+1} + c_{J+1} P_{J+2} = D_{J+1} \tag{59}$$

Solving Eq. (58) for P_J yields

$$P_J = E_{J+1} P_{J+1} + Q_{J+1} \tag{60}$$

where

$$E_{J+1} = -\frac{c_J}{b_J} \quad ; \quad Q_{J+1} = \frac{D_J}{b_J} \tag{61}$$

Substituting Eq. (60) for P_J into Eq. (59) gives

$$a_{J+1}(E_{J+1} P_{J+1} + Q_{J+1}) + b_{J+1} P_{J+1} + c_{J+1} P_{J+2} = D_{J+1} \tag{62}$$

Solving for P_{J+1} yields

$$P_{J+1} = E_{J+2}P_{J+2} + Q_{J+2} \tag{63}$$

where

$$E_{J+2} = -\frac{c_{J+1}}{b_{J+1} + a_{J+1}E_{J+1}} \quad ; \quad Q_{J+2} = \frac{D_{J+1} - a_{J+1}Q_{J+1}}{b_{J+1} + a_{J+1}E_{J+1}} \tag{64}$$

In general, the following recursion formulas are valid:

$$P_j = E_{j+1}P_{j+1} + Q_{j+1} \tag{65}$$

where

$$E_{j+1} = -\frac{c_j}{b_j + a_jE_j} \tag{66}$$

$$Q_{j+1} = \frac{D_j - a_jQ_j}{b_j + a_jE_j} \tag{67}$$

It is assumed that the right-hand boundary at j = M, k = K is also a closed boundary, as shown in Fig. 3.

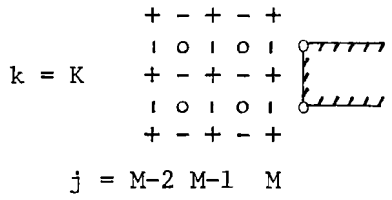

Fig. 3--Right closed boundary

The advective and diffusive transport of constituent i through the cross section between j = M and j = M + 1 is zero for this case, and therefore $c_M \equiv 0$. Equation (57) for j = M then becomes

$$a_MP_{M-1} + b_MP_M = D_M \tag{68}$$

and solving for P_{M-1} yields

$$P_{M-1} = -\frac{b_M}{a_M} P_M + \frac{D_M}{a_M} \tag{69}$$

Writing the general recursion formula given by Eq. (65) for j = M - 1 leads to

$$P_{M-1} = E_M P_M + Q_M \tag{70}$$

Using Eq. (70) in Eq. (69) gives

$$E_M P_M + Q_M = -\frac{b_M}{a_M} P_M + \frac{D_M}{a_M} \tag{71}$$

and solving for P_M yields

$$P_M = \frac{D_M - a_M Q_M}{b_M + a_M E_M} \equiv Q_{M+1} \tag{72}$$

The recursion factors E and Q are calculated in ascending order, starting with E_{J+1} and Q_{J+1}, given by Eq. (61). Equations (66) and (67) are used to calculate the remaining recursion factors to j = M, noting that $E_{M+1} \equiv 0$ since $c_M = 0$. The concentrations are then computed in descending order, starting with j = M, using Eq. (65).

If instead of a closed boundary at either end of the computational field, the geography of the region to be modeled requires an open boundary, then the above procedure must be modified slightly. As in the example given for the flow model, it is assumed that part of the left-hand boundary, j = 1, of the computational field contains an open boundary, as shown in Fig. 4. For this case, E_2 is set equal to zero and Q_2 is set equal to the concentration of constituent i at the open boundary, P_1. This concentration is a given input variable and is

usually a function of time. The methods used to obtain P_1 for the sample calculations are explained in the next section.

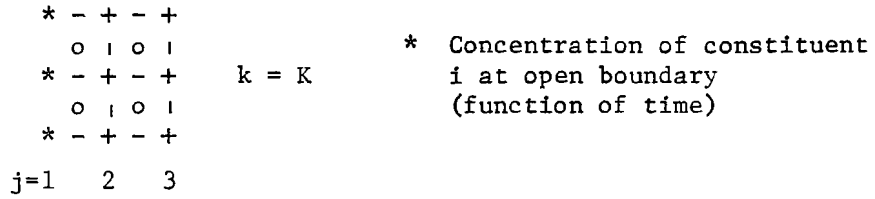

Fig. 4--Left open boundary

The rest of the recursion factors and concentrations are then calculated in the same way as for a closed boundary.

VI. OPEN BOUNDARY CONDITIONS AND TIDAL-FLAT COMPUTATIONS

The numerical procedures used at the major land-water boundaries in the flow model are those described in Refs. 1 and 3. These boundaries are taken through lines at the locations of the water depths so that the local velocity components are set to zero. Revisions and major additions have been made in the procedures used to describe the changing location of the land-water boundaries near tidal flats and marshy areas. These procedures are described in detail in this section. In addition, the methods used to approximate the open boundary condition in the mass-transport model are discussed.

TIDAL-FLAT COMPUTATIONS

In estuaries with large areas of shallow water and a significant tidal range, many marshes alternately dry and flood with each tidal cycle. In the development of the flow model, this was simulated by making the location of the land-water boundary a function of the current value of the depth, thus simulating the changing boundary during rising and falling tides.

To help describe the procedures used to determine the new land-water boundaries, several volumetric and area flow quantities must be defined. A representative portion of the staggered grid network is shown in Fig. 5. For convenience, it is assumed that the grid network is oriented so that the y coordinate lies along the northward direction.

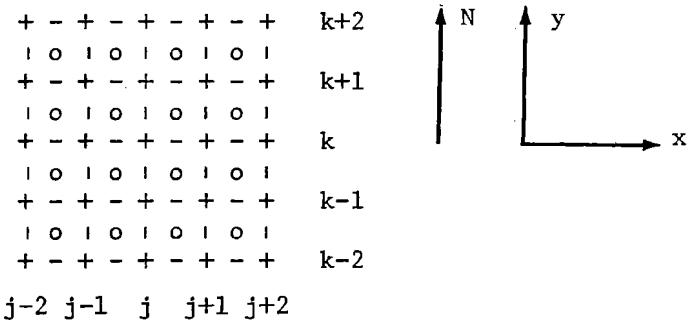

Fig. 5: Representative grid network

The volume element of water associated with each grid point j,k at time level n is defined as

$$VOL^{n}_{j,k} = \left[\zeta^{n}_{j,k} + \frac{1}{4}\left(h_{j-\frac{1}{2},k-\frac{1}{2}} + h_{j-\frac{1}{2},k+\frac{1}{2}} + h_{j+\frac{1}{2},k-\frac{1}{2}} + h_{j+\frac{1}{2},k+\frac{1}{2}}\right)\right](\Delta x)^2 \tag{73}$$

To describe the transport of constituents from one grid point to another, one must define a transport cross section. The cross section for transport in the eastward or westward direction between grid points j,k and j+1,k at time level n is

$$\frac{1}{2}\left(\zeta^{n}_{j+1,k} + \zeta^{n}_{j,k} + h_{j+\frac{1}{2},k+\frac{1}{2}} + h_{j+\frac{1}{2},k-\frac{1}{2}}\right) \tag{74}$$

The three transport cross sections for flow between grid point j,k and the other three surrounding grid points are defined in a similar manner. The Chezy coefficient, C, which is computed at each water-level location (as described in Ref. 1), is used as an indicator to designate whether a particular grid point is dry or wet. A value of C = 0 indicates land, while a positive value designates water.

There are several methods by which a grid point that is currently wet can become dry. The first check is made after each calculation of a new water level. If at a particular grid point, the new computed value of the water level has decreased so that a negative volume is obtained, then that grid point is taken out of the computation. This is accomplished by setting to zero the Chezy coefficient and the current values of the velocity components leading to that grid point. In addition, to correctly simulate the new land point in the computation of adjacent water levels and velocities, the previous row or column of recursion formulas, velocities, and water levels is recalculated with the point now taken as dry. For example, if during the solution of Eqs. (26) and (31) at time level n along row k, the computation of $\zeta^{n+\frac{1}{2}}_{j,k}$ leads to a negative value for $VOL^{n+\frac{1}{2}}_{j,k}$ as given by Eq. (73), then $C_{j,k}$, $v_{j,k+\frac{1}{2}}$, $v_{j,k-\frac{1}{2}}$, $u_{j+\frac{1}{2},k}$, and $u_{j-\frac{1}{2},k}$, are all set to zero. The

program then repeats the calculation of all velocities and water levels along row k-1 using the new land values for grid point j,k. In addition, the calculation of all velocities and water levels along row k is repeated before the computation proceeds to row k+1.

As a point is allowed to become dry, it is assumed that a thin layer of still water will remain over it. The thickness of this layer is set equal to the water level calculated at the previous time step, since this calculation did not lead to a negative volume element. Thus conservation of water mass throughout the computational field is maintained. In this still water, reactions between constituents and decay or buildup of constituents which occur in the main body of fluid will continue. All flow processes are eliminated in these tidal-flat areas.

The constituent reactions in the tidal-flat areas are simulated by solving Eq. (57) in the same way as described in Section V of this Report. The only difference is that when the constituent concentration is computed for a grid point with $C \equiv 0$, i.e., a dry point, all terms involving velocities and diffusion coefficients in Eq. (57) are set to zero. Thus, $a_j = 0$ and $c_j = 0$, while b_j is given by Eq. (55) with only the first, second, and seventh terms present, and D_j is given by Eq. (56) with the second through fifth terms set to zero. The computation is then carried out exactly as described in Section V. By simulating the constituent concentration present in the tidal flats and allowing for reactions to occur, the constituent mass is conserved throughout the region of the computation.

The second check on the possibility of a grid point becoming dry is made before the calculation of the advective and dispersive transport of constituents throughout the fluid. Transport cross sections are first computed using the newly calculated water levels from the flow computation. Before the calculation of the new constituent concentration, a check is performed on all four transport cross sections associated with each of the four adjacent grid points. If any of the cross sections are negative, a counter is set and the location of the grid point retained. A negative cross section is impossible physically, and leads to constituent transport in the direction opposite to what it should be, as shown by Eq. (51). At the end of the computation of the

constituent transport and new concentrations, the C values at these points and all velocities leading to these points are set to zero. Again a thin layer of water equal to the current value for the water level at these points is allowed to remain, and the reactions among constituents are simulated as described above. Thus water and constituent mass are conserved.

It should be noted that at time level n, only those cross sections associated with the diffusive transport terms in Eq. (51) use the newly computed water-level values, i.e., $\zeta^{n+\frac{1}{2}}$. If these cross sections are negative they are set to zero before the new constituent computation is carried out. This is a good approximation, however, since diffusive transport represents only a small percentage of the total transport. The main contribution is given by the advective terms, and these are computed using water levels and cross sections at time step n, for which a check on negative cross sections has already been made.

Since it is numerically possible for a negative volume or a negative cross section to be calculated at any time step throughout the computation, the above two checks are made at each time step to avoid incorrect transport of water and constituent mass. Thus discrete changes in the system boundaries can occur at each time step. Even though the application of finite-difference approximations usually depends on representing functions with variables slowly varying in time and space, it is found that the discrete changes made in the shape of the boundaries of the tidal flats during the computation do not lead to the generation of any instabilities or discontinuities. One of the reasons for this is that the possible occurrence of a large number of boundary changes in succeeding time steps is reduced by using the original boundary-change procedures described in Ref. 1. For this case, the procedure is as follows. If at a particular grid point, any of the four transport cross sections (where one uses only the water level at the grid point rather than an average) decreases to less than a preset value, then that grid point is taken out of the computation. Since the preset value is always greater than zero, this is a more restrictive condition than the two described above. The water level is set at its current value and is maintained at this level until the point floods. Reactions among constituents continue as described previously.

To suppress the effect of the generation of disturbances due to discrete changes in the boundaries, this cross-section search is made at intervals larger than the time step so that the computational noise generated by the boundary change decays. By searching at intervals larger than the time step and by using a more restrictive condition, it is found that a large proportion of the boundary changes are made by this procedure, while only a few changes occur because of negative volumes or negative cross sections. In this way, the effect of local discontinuities generated by the discrete boundary changes is decreased.

The flooding procedure is very similar to that described in Ref. 1, with the exception of several important additions. Each of the four surrounding grid points adjacent to a dry grid point is checked to see whether it is under water. If one or more of the surrounding grid points are wet, then the water levels of those surrounding grid points that are under water are averaged. If this average water level is larger than the water level retained on the dry grid point, then the grid point may be allowed to flood. First a check is made on the transport cross sections between the dry grid point and each of the surrounding grid points that are under water. If any of these cross sections are negative, the point remains dry. If all are positive, then the grid point is allowed to flood, and it is added back to the computational field. The water level is set at the value which was allowed to remain over the grid point when it became dry, and the constituent concentration is that which has resulted from the calculation of the reactions which occur on the tidal flats. This procedure preserves the conservation of water and constituent mass.

Flooding can occur from one to four sides of the grid point, and when flooding occurs from one to three sides there are many different combinations possible. All these possibilities must be explored during the determination of the new boundary. The check for flooding is also made at intervals larger than the time step, to reduce the effect of the discrete boundary-condition change when a grid point is added back into the computation.

OPEN BOUNDARY CONDITIONS

As an illustration, an open boundary has been assumed along part of the west side of the computational field. At the open boundary, the water levels, $\zeta_{1,k}^{n+\frac{1}{2}}$, are given input values for the flow computation. These are time varying according to the input tide. One can prepare input tables that give water levels at each time step, or, as in the case of the present model, at every third time step with a linear interpolation between. The current at the open boundary is taken to be in the eastward or westward direction with zero vertical components. Thus the velocity components, $v_{1,k}^{n}$ and $v_{1,k-1}^{n}$ are taken to be zero.

Since horizontal velocities outside the computational field are not known, the advective term in the momentum equation is assumed to be zero at the open boundary. Equation (19) then takes the form

$$\delta_t u - f\bar{v} + \overline{\bar{v}\delta_y u}^{y} + g\delta_x \zeta^{t} + g\,\frac{\bar{u}^{t}\left[(u_{-})^2 + (\bar{v})^2\right]^{\frac{1}{2}}}{(\bar{h}^{y} + \bar{\zeta}^{x})(\bar{C}^{x})^2} - \frac{1}{\rho(\bar{h}^{y} + \bar{\zeta}^{x})}\,\tau_x^{s} = 0$$

at $j+\frac{1}{2}$, k, n (75)

This equation, along with the continuity equation, is solved in the same manner as described in Section IV, with one minor change. The variable $r'_{j+\frac{1}{2}}$ given by Eq. (33) becomes

$$r'_{j+\frac{1}{2}} = 1 + \frac{g\Delta t}{2}\,\frac{\left[(u_{j+\frac{1}{2},k}^{n-\frac{1}{2}})^2 + (\bar{v})^2\right]^{\frac{1}{2}}}{(\bar{h}^{y} + \bar{\zeta}^{x})(\bar{C}^{x})^2} \qquad (76)$$

and the wind-stress term in Eq. (34) has been omitted.

At the open boundary of the model, the concentrations of the various constituents must be described as a function of time. During outflow, the boundary concentrations are obtained by linearly extrapolating from the values computed inside the computational field. Thus the new concentrations at the boundary are given by

$$P^{n+\frac{1}{2}}_{1,k;i} = P^{n}_{1,k;i} - u^{n+\frac{1}{2}}_{1+\frac{1}{2},k} \left(P^{n}_{2,k;i} - P^{n}_{1,k;i}\right) \frac{\Delta t}{2\Delta x} \qquad (77)$$

In this approximation, only transport of constituents by advection to the boundary is simulated, and thus it should be used only in estuaries or bodies of water where dispersive transport is small. If dispersive transport is significant, it can be easily incorporated into the boundary conditions of the present model.

As the tide changes and flow returns into the estuary, the constituent concentration at the boundary can no longer be determined from values inside the computational field. Here it is assumed that the boundary value of the concentration either increases or decreases to some preset input value over a specified period of time (which can be varied). The functional relationship describing the variation in concentration from the slack-water value to the preset value is arbitrary. A half-cosine variation is currently used; however, this can be changed if field measurements indicate the appropriateness of other functional relationships. Once the preset boundary value is reached, it remains constant until outward flow begins, at which time the boundary value is again obtained by extrapolation from inside the computational field.

It should be emphasized here that the above methods for describing the constituent concentration at an open boundary are approximations which are found to be valid for the bays and estuaries we are studying. Other areas may present different hydraulic or geographic conditions which require the application of other boundary conditions. The general flexibility of the model allows for variations to satisfy the appropriate boundary conditions.

VII. DATA PROCESSING

The preceding sections of this Report, contain a description of the numerical procedures used to solve the momentum and continuity equations of fluid flow, along with constituent mass-balance equations, to obtain the time and space distribution of waste constituents in bays or estuaries. This analysis has led to the development of an extensive computer program, which is presently being used and evaluated in a study of the current and projected water quality of Jamaica Bay, New York.

Since the problem is time-dependent and attempts to simulate real-world conditions, large numbers of input data describing the characteristics of the area to be studied are required. In addition, the results of the computation can be presented at every grid point and at each succeeding time step. However, interpreting and extracting important results from such a large volume of printed numerical data rapidly becomes impossible. Thus, several routines using interactive computer technology were developed for data insertion, and programs were written to generate machine-made drawings for graphical presentation of the results of the computation. These input and output procedures are described in the following subsections.

HYDRAULIC FLOW MODEL

Inputs

Bathymetry. Depth data or elevation above mean sea level (values for h) are input at each grid point within the field. For the Jamaica Bay Model a grid size of 500 ft was selected, which gives rise to a data array of 78 by 61 points. One array is used for the depth and elevation data, and this information is read in from cards. If no data are inserted at a particular grid point, land is assumed.

Determination of land-water boundary. The procedures used to determine the land-water boundary are described in Section VI of this Report. The boundary location is dependent upon the tide stage, and is thus time varying. One data array is used to store the water level that remains on the tidal-flat areas as they become dry.

Open boundaries. At present, open boundaries are permitted only along the west side of the computational field. At the open boundary, a time history of the water level is given as a function of the input tide. The input water levels are given at every third time step, with a linear interpolation used between. Since real-time simulations of several days are desired in many cases, the number of input data can become excessive. To facilitate this data insertion, a computer program was written for use with the Rand Tablet,[4] a graphic computer input device used in conjunction with a computer and oscilloscope display.[5] The advantage of this system is that graphical information, such as water-level time histories, can be transformed directly into digital information by tracing over the curves with a stylus. The digital information is then punched directly onto cards in the format desired for the input data.

Latitude. The latitude is given in degrees of the center of the area of computation. The effect of a variation in the Coriolis acceleration over the area of a very large body of water is not simulated in the present program.

Manning's value and/or Chezy value. The investigator has the option of defining a Chezy value over the entire field or computing periodically a value from Manning's n (which is variable over the field) as a function of the water level (see Ref. 1, page 7). Two data arrays are used to store the appropriate Manning's n input value and the time-and-space dependent Chezy coefficient. If a specific value is not inserted or computed, a default value is used.

Atmospheric inputs. Wind speed and direction are inserted as a function of time so that the wind-stress term in the momentum equation can be determined. Future development of the model may require the time histories of rainfall and evaporation as well as air-pressure differences.

Location of discharge points. Time histories of the fluid discharges at the locations of the outfalls of sewage-treatment plants and combined sewer overflows are input. At present, only point sources at the outfalls are provided for.

Outputs

Velocities and water levels. Four types of output presenting velocity and water-level data can be obtained from the simulation model.

1. Graphs. Using the Integrated Graphics System,[6] graphic output giving velocity vectors and water levels at selected points and times can be made on film or as hard copy using an SC-4060. Figure 6 is a sample of this type of output for the Jamaica Bay model. This graphic output displays the outline of the bay at the approximate location of the high-water line and the grid points at which the water levels and constituent mass densities are computed. As the water level in the marshy areas changes with time, the number of points in the computation varies, since some areas become dry while others flood. The blank areas with no (.) indicate land. Thus the changing location of the land-water boundaries can be easily followed.

Velocity vectors are computed at the location of the water levels from the average of the surrounding u and v components. These vectors are plotted at every second grid point in the x and y directions. Water levels are printed out at selected locations in the bay. These locations, marked by an X, are variable, and the water-level information is printed below and to the right of the X. The locations of the outfalls of sewage-treatment plants are marked with an O, and combined storm-water/sewage-overflow locations are marked with a V.

The graphic output can be obtained at any interval desired. Normally, records are made every one or two hours of real time. If the graphs are printed at each time step, one can make a 35-mm movie showing the time variation of the velocity vectors over the area of the bay.

2. Numerical velocity and water-level data. Printed numerical data of the water levels and the u and v velocity components at each point on the grid can be obtained at selected time intervals. Again, these data are usually printed out every one or two hours of real time.

3. Velocity and water-level time histories. The velocities and water levels at selected points in the bay are graphed as a function of time using the computer graphics system. Sample outputs of this type for the Jamaica Bay Study are shown in Figs. 7 and 8. To enhance

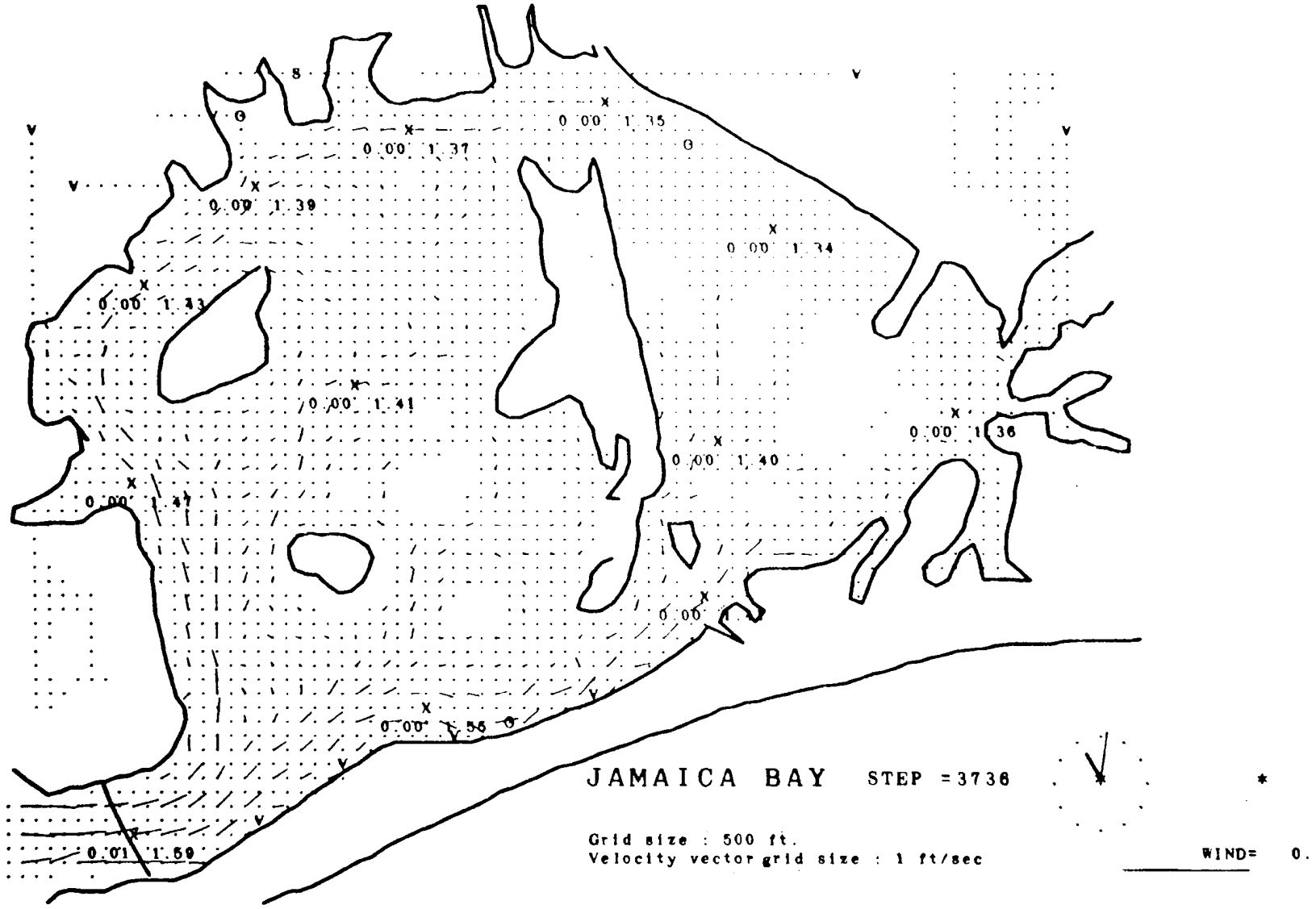

Fig. 6 — Velocity vectors and water levels

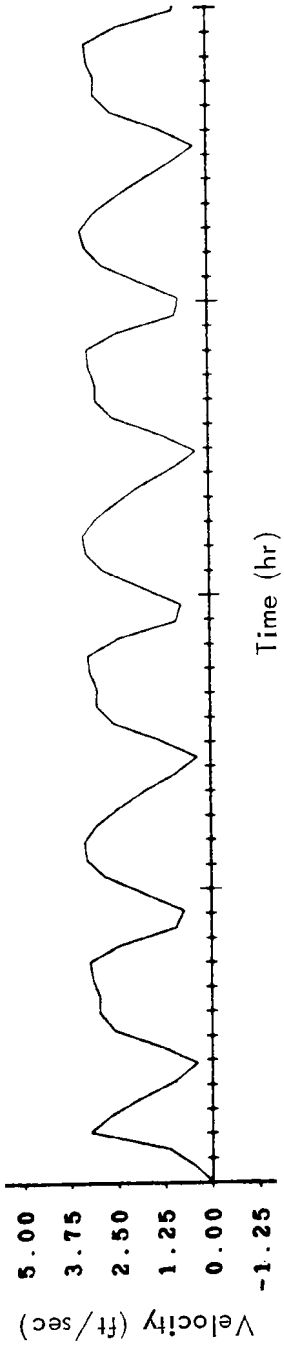

Fig. 7 — Time history of the magnitude of the water velocity at a selected location

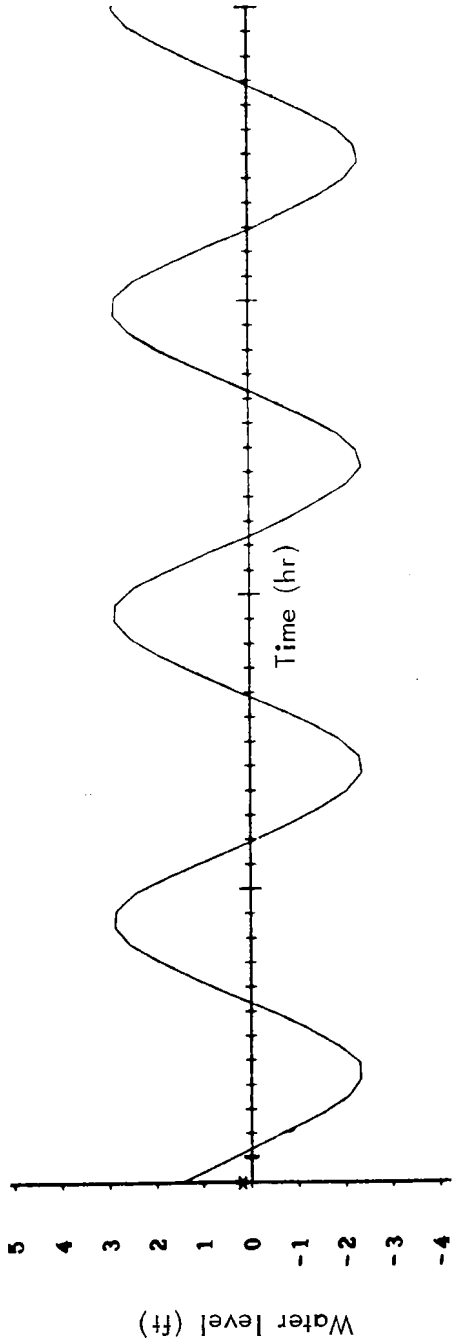

Fig. 8 — Time history of the water level at a selected location

the visual presentation of these results, the data are smoothed in time before the computer graphs are made. This is done in a temporary storage location, so that it does not affect the subsequent results of the computation.

4. Water-level field information at specific times. It is possible to obtain water-level isocontours of the water-level information in graphical form as described in 1 above. In addition, a three-dimensional view of the water levels can be produced using the computer graphics system.

Future extensions of this type of output will allow isocontours of the maximum velocities and/or velocity components to be produced and presented on graphs similar to Fig. 6.

The output forms described in 3 and 4 above are obtained by processing data generated by the model, which are initially written on tape. In the flow computation, two data arrays are used for each of the two velocity components and three arrays for the water levels, since three time levels are involved.

Water mass transport through sections. The circulation of fluid generated by the tide in a bay or estuary is one of the major mechanisms by which constituents are transported. To determine the direction and magnitude of this circulation, it is important to know the integrated mass transport of fluid through various sections in the bay. The locations of the cross sections used in the Jamaica Bay Study are shown in Fig. 9. Each section is located in a north-south direction. Future additions will provide for east-west cross sections as well.

The advective or flow transport of fluid across a north-south plane in an east-west direction at $j+\frac{1}{2},k$ and time level n is given by

$$(HUdy)^n = \left[\frac{1}{2}(\zeta^n_{j,k} + \zeta^n_{j+1,k}) + \frac{1}{2}(h_{j+\frac{1}{2},k+\frac{1}{2}} + h_{j+\frac{1}{2},k-\frac{1}{2}})\right] u^{n+\frac{1}{2}}_{j+\frac{1}{2},k}\ \Delta y \qquad (78)$$

and at time level $n+\frac{1}{2}$ it is

$$(HUdy)^{n+\frac{1}{2}} = \left[\frac{1}{2}(\zeta^{n+\frac{1}{2}}_{j,k} + \zeta^{n+\frac{1}{2}}_{j+1,k}) + \frac{1}{2}(h_{j+\frac{1}{2},k-\frac{1}{2}} + h_{j+\frac{1}{2},k+\frac{1}{2}})\right] u^{n+\frac{1}{2}}_{j+\frac{1}{2},k}\ \Delta y \qquad (79)$$

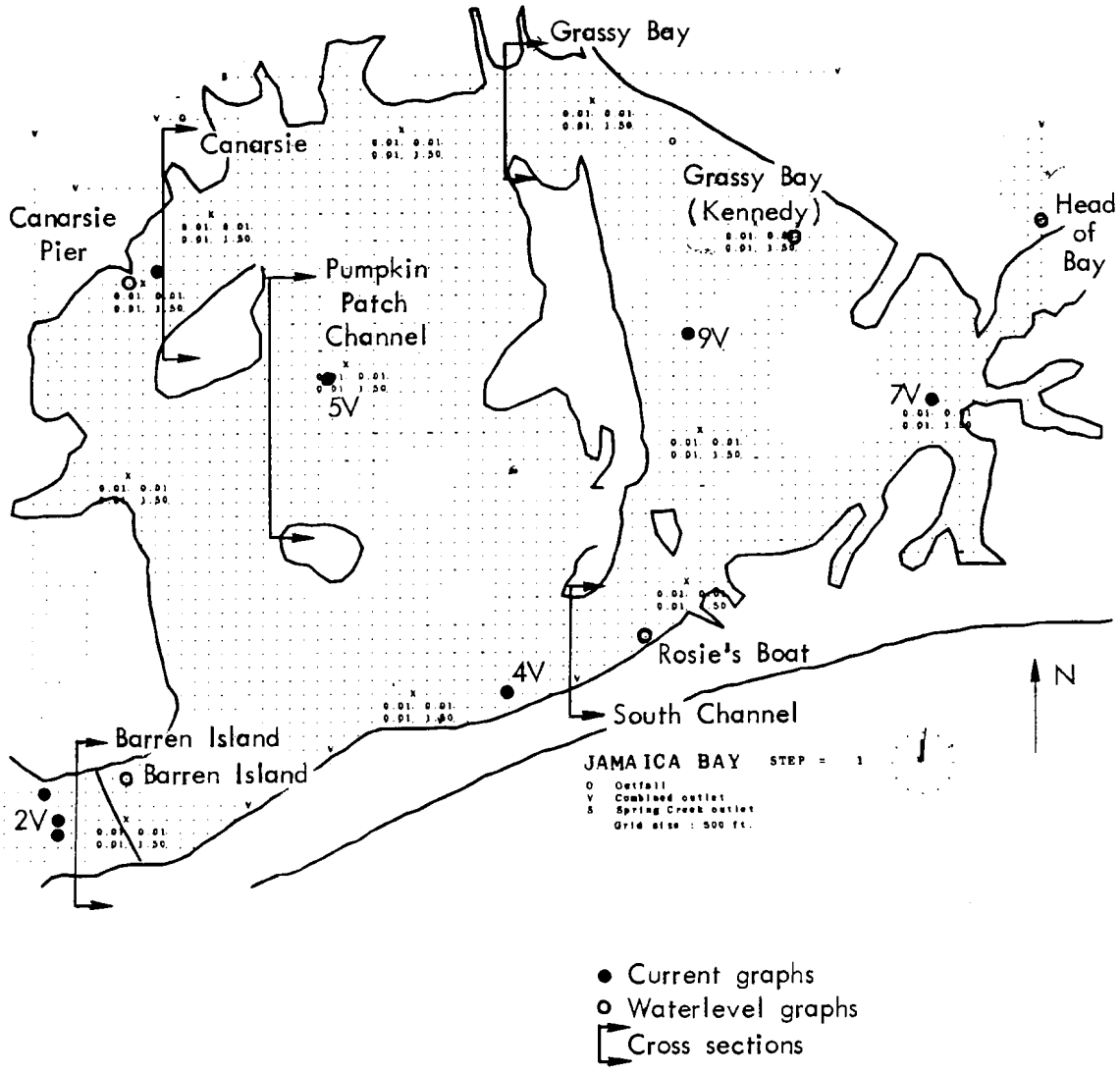

Fig.9 — Location of verification data points in the model

where $\Delta y = \Delta x$ for a square grid. Thus, the average advective transport over a full time step is

$$\overline{HUdy}^{t/2} = \frac{1}{2}\left[(HUdy)^n + (HUdy)^{n+\frac{1}{2}}\right]$$

$$= \left\{\frac{1}{2}(\zeta^{n+\frac{1}{2}}_{j,k} + \zeta^{n+\frac{1}{2}}_{j+1,k} + \zeta^{n}_{j,k} + \zeta^{n}_{j+1,k}) + (h_{j+\frac{1}{2},k+\frac{1}{2}} + h_{j+\frac{1}{2},k-\frac{1}{2}})\right] u^{n+\frac{1}{2}}_{j+\frac{1}{2},k} \frac{\Delta x}{2} \qquad (80)$$

The total integrated transport of fluid through a north-south cross section between k_{min} = NIT1 and k_{max} = NIT2 is found to be

$$T_f = \sum_{n=0}^{nmax} \sum_{k=NIT1}^{NIT2} \left[\frac{1}{2}(\zeta^{n+\frac{1}{2}}_{j,k} + \zeta^{n+\frac{1}{2}}_{j+1,k} + \zeta^{n}_{j,k} + \zeta^{n}_{j+1,k}) + (h_{j+\frac{1}{2},k+\frac{1}{2}} + h_{j+\frac{1}{2},k-\frac{1}{2}})\right] u^{n+\frac{1}{2}}_{j+\frac{1}{2},k} \frac{\Delta t \Delta x}{2} \qquad (81)$$

where the total time interval is nmax · (Δt). An illustrative example of the computed water transport for the Jamaica Bay Study is shown in Fig. 10.

ADVECTIVE-DIFFUSIVE TRANSPORT MODEL

Inputs (except those generated by the flow model)

Constituent time histories at open boundaries. The concentration of each of the constituents is described as a function of time at the open boundaries of the model, using the methods outlined in Section VI.

Concentration of the constituents in discharges. The concentration of each of the constituents, P_1 . . ., P_n, in the fluid discharges at the outfalls of the sewage treatment plants and combined sewer overflows is input as a function of time. Again, if the number of data warrant, this can be accomplished with the aid of the Rand Tablet.

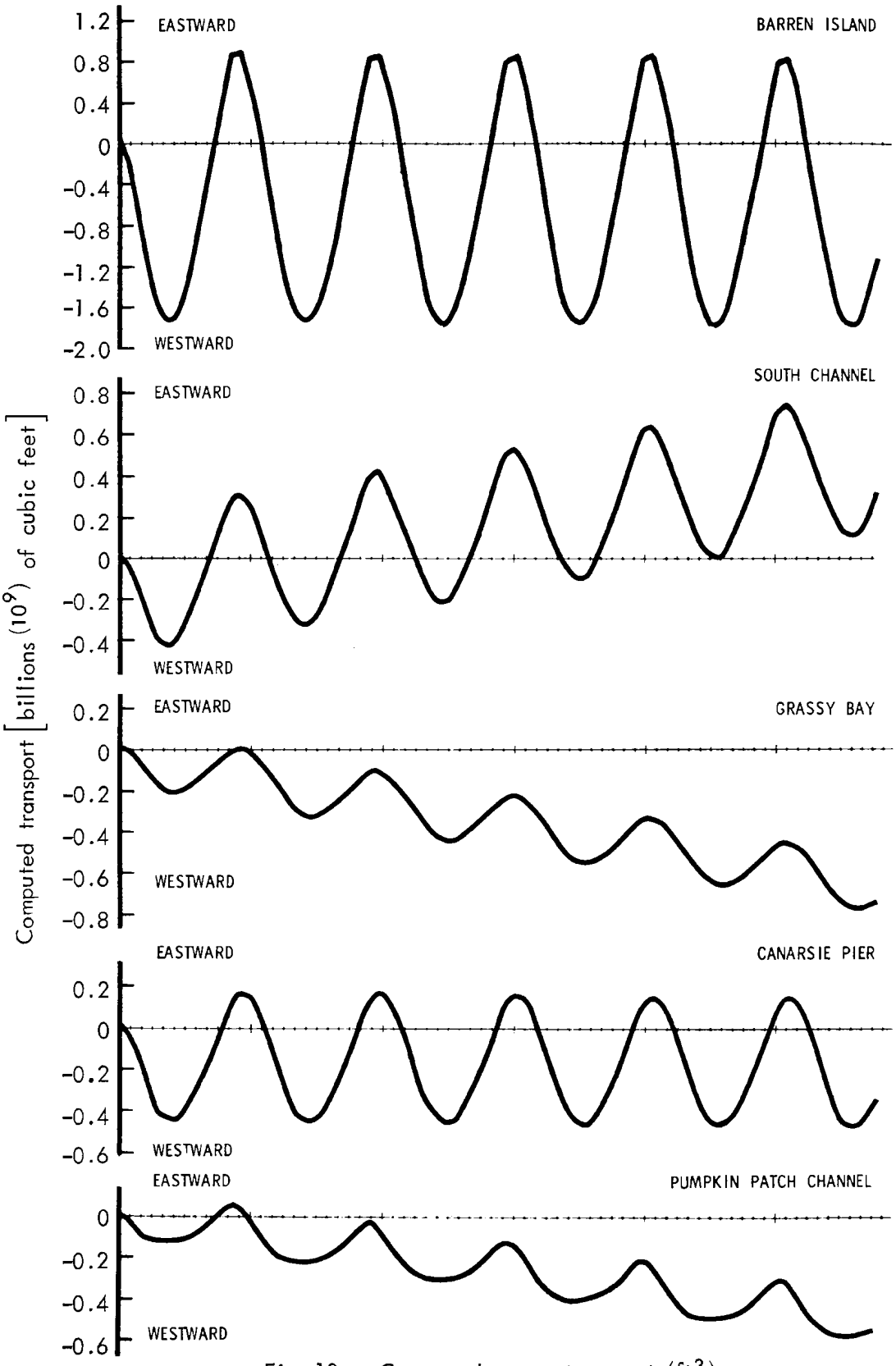

Fig. 10 — Computed water transport (ft^3)

Dispersion coefficients. The dispersion coefficient is composed of several terms as described in Ref. 1. First, a term dependent on lateral dispersion is input at every point in the field. If it is not specified at a particular point, then a default value is used. A second term is then computed as a function of the velocity component, depth, and Chezy coefficient, so that the total coefficient is time varying. Future additions to the model will allow for a term that is variable, depending upon wind conditions (gross effect only). One data array is used for the calculation and storage of the dispersion coefficient.

Initial constituent concentrations throughout the field. At the beginning of the computation, initial values of the constituent concentrations at each grid point are input. If these values are not given, a specified default value is used.

Outputs

Graphs. The mass densities of the constituents are plotted on graphs by means of isocontour lines. These graphical data are generally combined with the output of the flow model as described previously. A sample of this type of output, illustrating the distribution of salinity in Jamaica Bay, is shown in Fig. 11. If this output is obtained at every time step, an animated 35-mm movie results.

The subroutines that were developed to draw these isocontours are very complex, since at each grid point the concentration at surrounding grid points must be checked to determine if the isocontour passes between these points. The techniques for drawing isocontours used here are similar to those presented in Ref. 7. But in the subroutines used here, a termination of the isocontour had to be made at the land-water boundary. Numerical values of the constituent concentration are printed out at selected locations in the field, marked with an X, and the values of the adjacent isocontour lines can be obtained by extrapolation. The numerical values of the constituent concentration are printed out below and to the left of the X, and the values of the contour lines are listed in the legends.

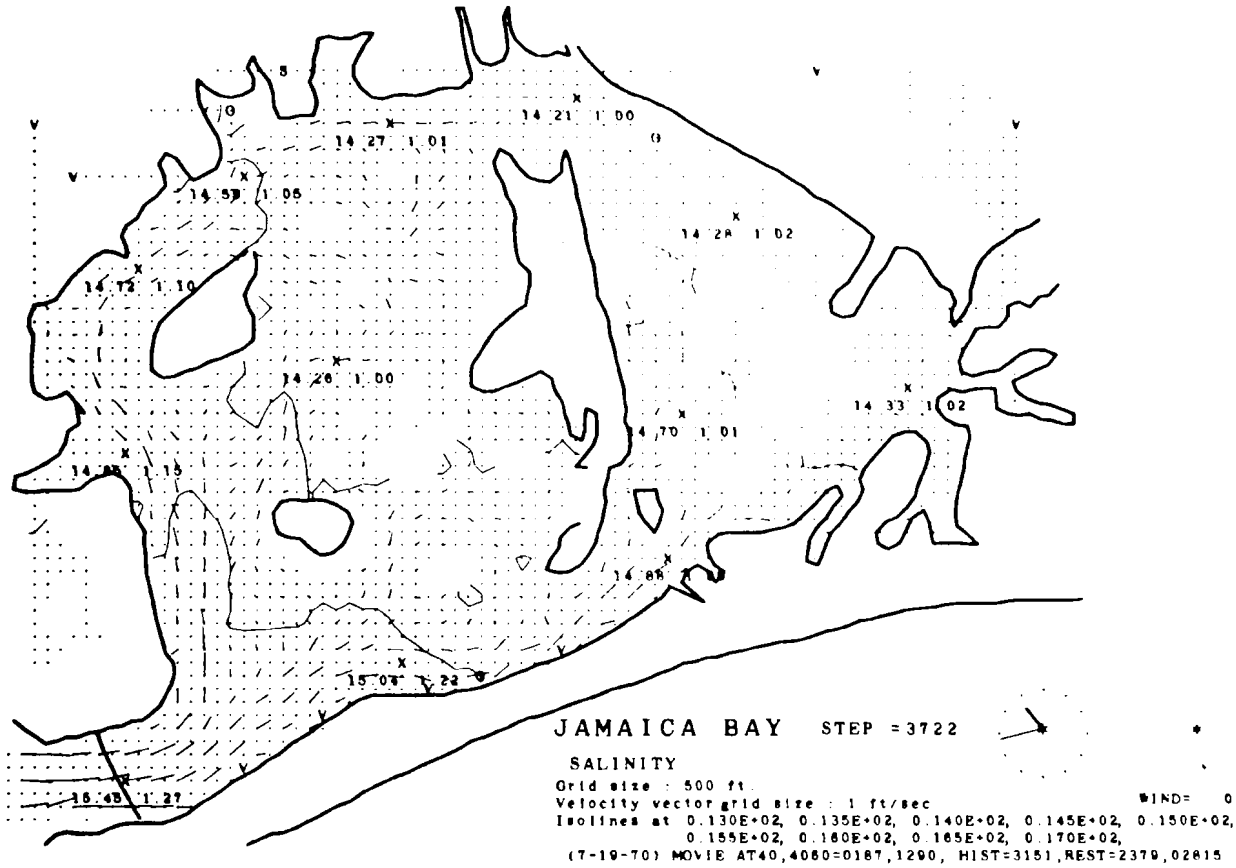

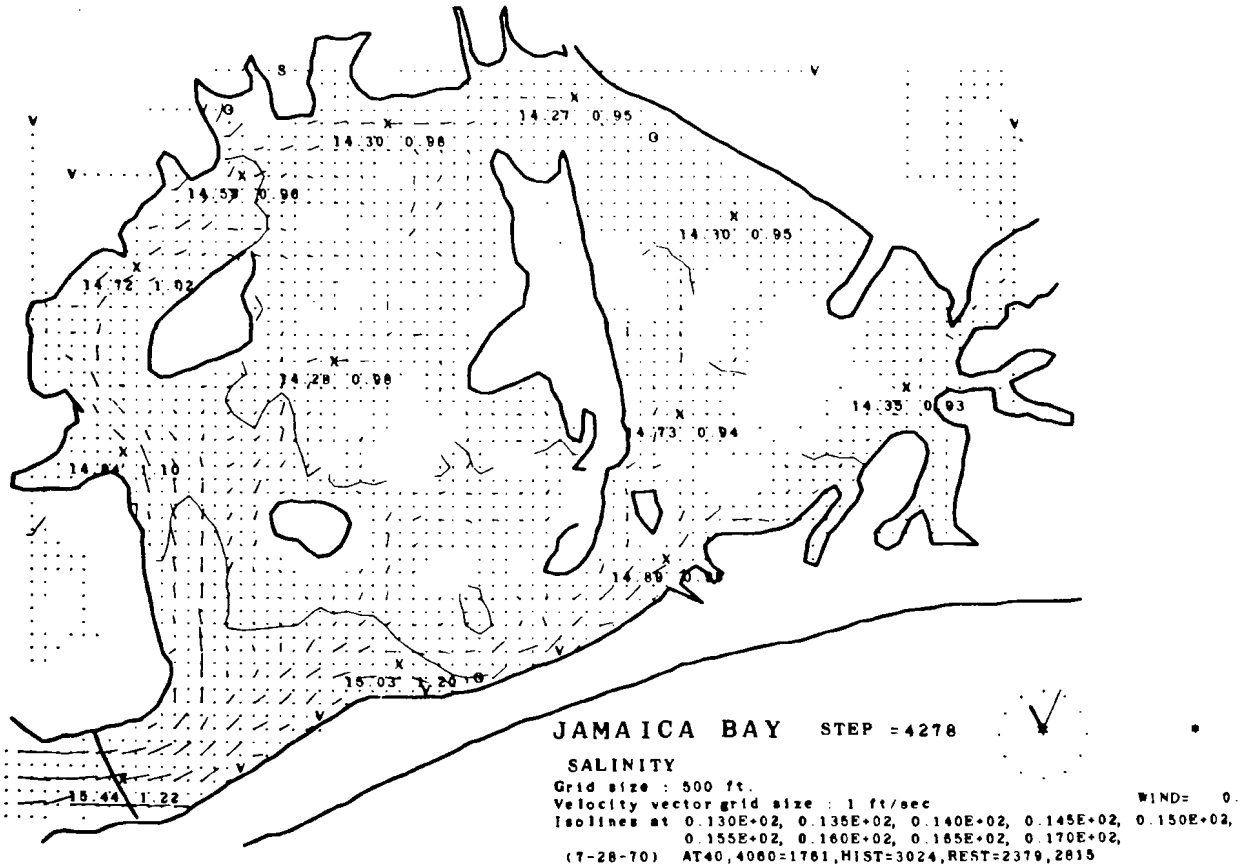

Fig.11—Distribution of salinity in Jamaica Bay at two times, one full tidal cycle apart

To improve the overall presentation of constituent concentration contours, the data were smoothed before the graphs were made. This was accomplished by using a temporary unused array for storage of the unsmoothed data, so that subsequent calculations are not affected by this smoothing operation. The amount of smoothing used is variable, with a minimum of no smoothing possible.

In the Jamaica Bay study, six constituents are computed simultaneously: dissolved oxygen (DO), biochemical oxygen demand (BOD), salinity, and coliform bacteria from three independent groups of sources. Twelve data arrays are used in the calculation of the constituents because of the two time levels involved.

Numerical values of the constituent concentration. Printed numerical data of concentrations of each of the constituents are obtained at each grid point. This information is printed out at the same time as the numerical velocity and water-level data.

Time histories of the constituent concentrations. The concentrations of the various constituents are graphed as a function of time at selected grid points in the bay. These data can then be compared with field measurements to ensure correct adjustment of the model. If necessary, these data can be smoothed as well. A sample output of this type, showing the time history of BOD at a specific grid point in the Jamaica Bay study, is shown in Fig. 12.

Constituent mass transport through sections. The total constituent mass transport is calculated at each of the cross sections through which water mass transport is computed. The diffusive and advective transport terms are computed and graphed individually, as well as their sum, so that the importance of each term can be determined.

The diffusive transport of constituent i across a north-south plane in an east-west direction at $j+\frac{1}{2},k$ over a full time step is given by

$$\overline{-HD\frac{\partial P}{\partial x}\,dy}^{t/2} = -\left\{\frac{1}{2}\left[\left(\zeta^{n+\frac{1}{2}}_{j,k} + \zeta^{n+\frac{1}{2}}_{j+1,k}\right) + \left(h_{j+\frac{1}{2},k-\frac{1}{2}} + h_{j+\frac{1}{2},k+\frac{1}{2}}\right)\right]\right.$$
$$\left.\times\, D^{n+\frac{1}{2}}_{x_{j+\frac{1}{2},k}}\left[\frac{1}{\Delta x}\left(P^{n+\frac{1}{2}}_{j+1,k;i} - P^{n+\frac{1}{2}}_{j,k;i}\right)\right]\right\}\Delta x \qquad (82)$$

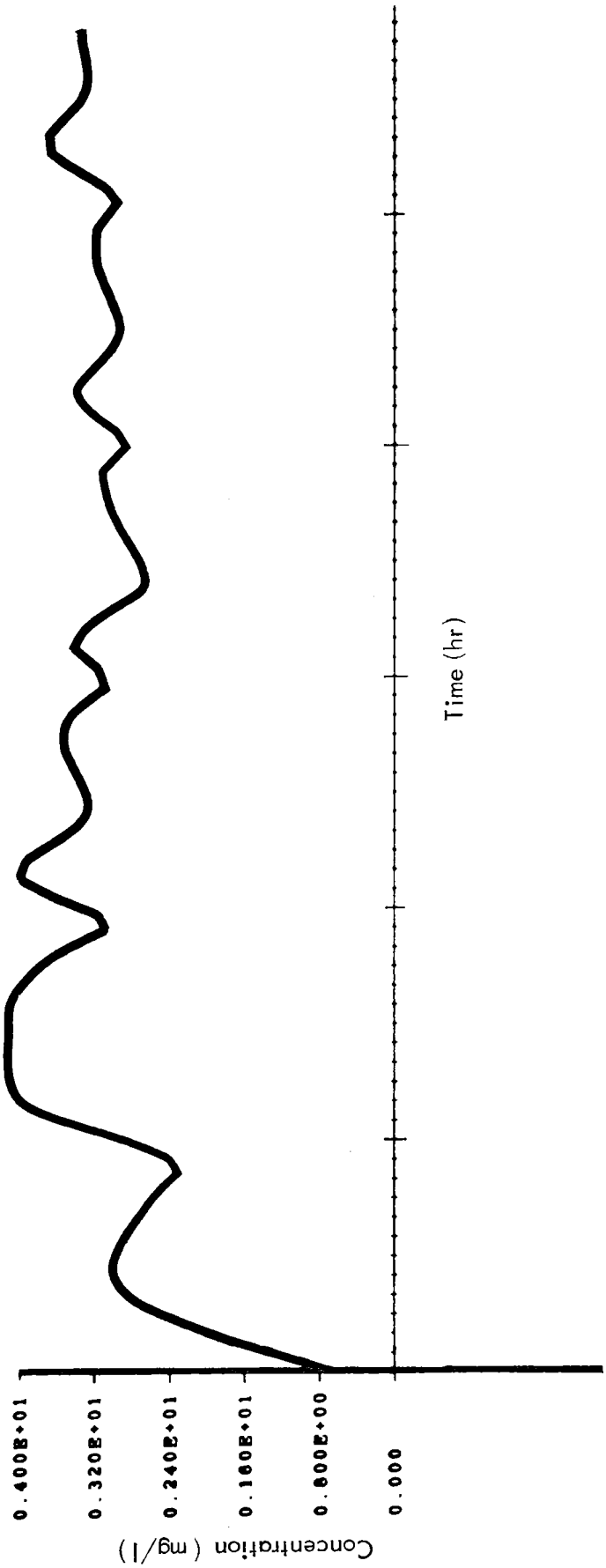

Fig. 12—Time history of the BOD concentration at a selected location

The total integrated diffusive transport of constituent i through a north-south cross section between k_{min} = NIT1 and k_{max} = NIT2 is

$$d_i = \sum_{n=0}^{nmax} \sum_{k=NIT1}^{NIT2} - \left\{ \left[\frac{1}{2} \left(\zeta_{j,k}^{n+\frac{1}{2}} + \zeta_{j+1,k}^{n+\frac{1}{2}} \right) + \frac{1}{2} \left(h_{j+\frac{1}{2},k-\frac{1}{2}} + h_{j+\frac{1}{2},k+\frac{1}{2}} \right) \right] D_{x_{j+\frac{1}{2},k}}^{n+\frac{1}{2}} \times \left[\frac{1}{\Delta x} \left(P_{j+1,k;i}^{n+\frac{1}{2}} - P_{j,k;i}^{n+\frac{1}{2}} \right) \right] \right\} \Delta x \Delta t \qquad (83)$$

where the total time interval is nmax · (Δt). The total integrated advective transport of constituent i is found in the same way as for the water-mass transport described above [see Eq. (81)], and is given by

$$A_i = \sum_{n=0}^{nmax} \sum_{k=NIT1}^{NIT2} \left\{ \left[\frac{1}{2} \left(\zeta_{j,k}^{n+\frac{1}{2}} + \zeta_{j+1,k}^{n+\frac{1}{2}} + \zeta_{j,k}^{n} + \zeta_{j+1,k}^{n} \right) + \left(h_{j+\frac{1}{2},k+\frac{1}{2}} + h_{j+\frac{1}{2},k-\frac{1}{2}} \right) \right] \frac{u_{j+\frac{1}{2},k}^{n+\frac{1}{2}}}{2} \left(P_{j,k;i}^{n+\frac{1}{2}} + P_{j+1,k;i}^{n+\frac{1}{2}} \right) \right\} \frac{\Delta t \Delta x}{2} \qquad (84)$$

In Fig. 13, an example of the type of constituent-transport results obtained in the Jamaica Bay study is shown, comparing the magnitude of the dispersive transport of DO to the corresponding advective transport. As can be seen, the advective transport is several orders of magnitude greater than the dispersive transport through this cross section, and therefore the total integrated transport (the sum of dispersive and advective) is essentially the same as the advective transport.

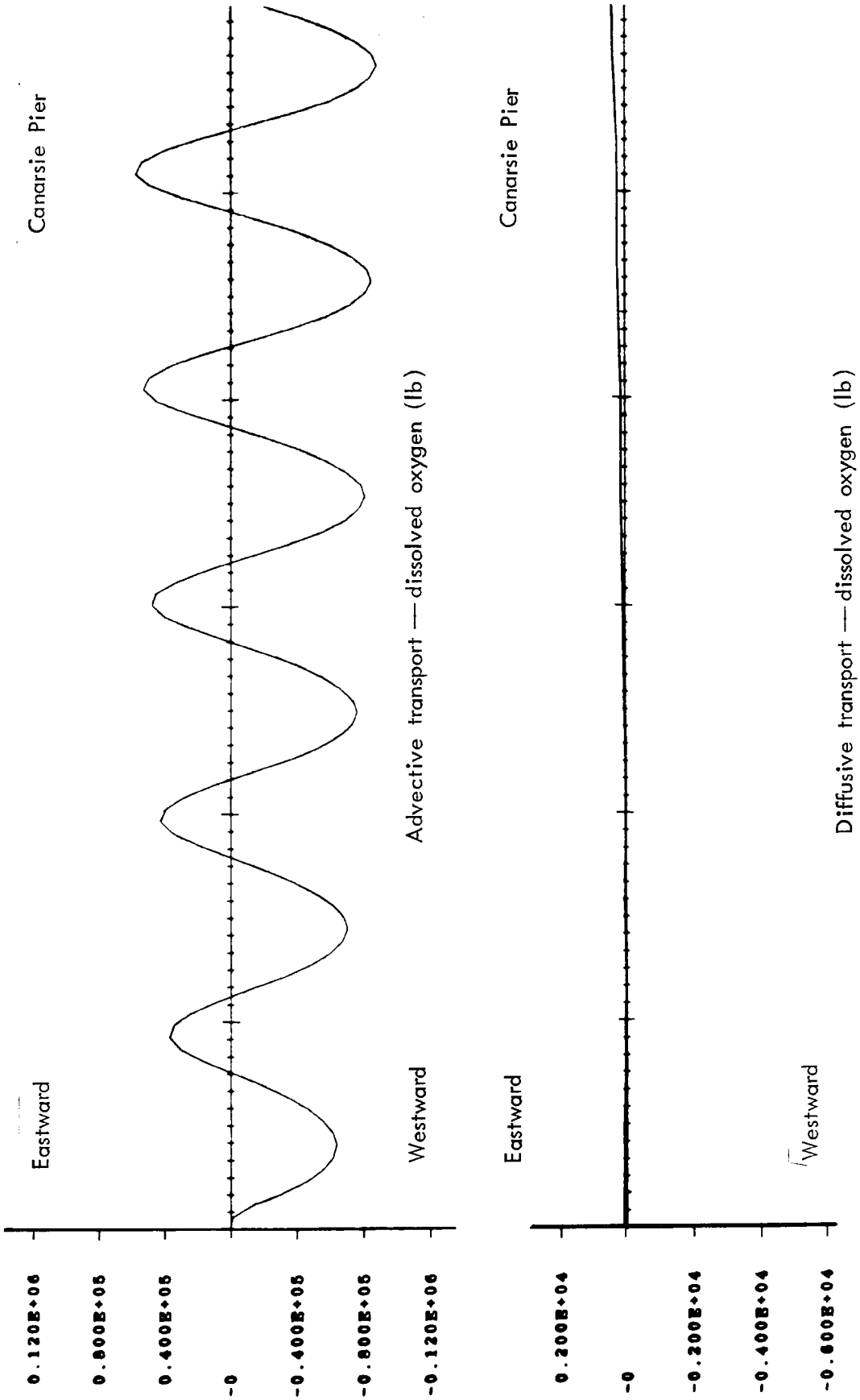

Fig. 13 — Mass transport of a constituent

REACTION MODELING

Inputs

Decay rates. The first-order decay constants for the coliform bacteria, K_{11}, K_{22}, and K_{33}, must be input. These values are determined experimentally from the decay rates obtained from field measurements.

First-order reaction rates. The reaction coefficient, K_{12}, in the BOD-DO reaction model is estimated from field measurements, and adjustments are then made to correctly simulate field data.

Source-sink functions. In the present model, this includes the reaeration coefficient of oxygen, K_{11}. This input value can currently be varied over the area of the computation. Future additions to the code will allow for a reaeration coefficient that is dependent upon the wind and wave conditions. This is necessary, since most bays and estuaries have very large surface areas that create a wind fetch distance large enough to generate substantial surface waves. These waves are then very important in the generation of turbulence at the surface, which affects the surface film replenishment rate, and in turn the reaeration coefficient.

If it is assumed that the oxygen mass-transfer coefficient is proportional to the wind energy dissipated within the fluid, which in turn is proportional to the length of fetch and the square of the wind velocity, then the wind-generated reaeration coefficient is

$$K_W = \varepsilon W^2 F \tag{85}$$

where

W = wind speed

F = fetch

ε = proportionality constant

In addition, the usual reaeration coefficient is included, based upon a rate of surface renewal dependent upon the surface turbulence generated

by the fluid velocity and bottom friction. This term has been shown in Ref. 8 to be given by

$$K_L = \frac{\sqrt{D_L (U^2 + V^2)^{\frac{1}{2}}}}{H^{\frac{1}{2}}} \tag{86}$$

where

D_L = molecular diffusivity of oxygen through the liquid surface

The form of the wind-, current-, and wave-dependent reaeration coefficient we propose to use for bays and estuaries is thus defined as

$$K_{11} = \frac{\gamma\sqrt{D_L (U^2 + V^2)^{\frac{1}{2}}}}{H^{\frac{1}{2}}} + \varepsilon W^2 F + \delta \tag{87}$$

The coefficients γ and ε allow the investigator to vary the importance of the current- and wind-generated terms of the reaeration coefficient to match field measurements. The term δ allows for reaeration in areas of the bay that are essentially unaffected by tidal motions and winds, and are essentially still bodies of water. The calculation of the fetch, F, is not a trivial matter, since land areas continually appear and disappear with the changing tide level. In addition, the wind direction is variable, so that these conditions lead to a time-varying fetch distance and reaeration coefficient. One data array is needed in the program for the reaeration coefficient.

REFERENCES

1. Leendertse, J. J., A Water-Quality Simulation Model for Well-Mixed Estuaries and Coastal Seas: Volume I, Principles of Computation, The Rand Corporation, RM-6230-RC, February 1970.

2. Dronkers, J. J., Tidal Computations in Rivers and Coastal Waters, North-Holland Publishing Company, Amsterdam, 1964.

3. Leendertse, J. J., Aspects of a Computational Model for Long-Period Water-Wave Propagation, The Rand Corporation, RM-5294-PR, May 1967.

4. Davis, M. R., and T. O. Ellis, The Rand Tablet, A Man-Machine Graphical Communication Device, The Rand Corporation, RM-4122-ARPA, August 1964.

5. Brown, G. D., and C. H. Bush, The Integrated Graphics System for the IBM 2250, The Rand Corporation, RM-5531-ARPA, October 1968.

6. Brown, G. D., C. H. Bush, and R. A. Berman, The Integrated Graphics System for the S-C 4060: Volume I, User's Manual, The Rand Corporation, RM-5660-PR, December 1968.

7. Murray, F. W., A Method of Objective Contour Construction, The Rand Corporation, RM-5564-NRL, February 1968.

8. O'Connor, D. J. and W. E. Dobbins, "Mechanism of Reaeration in Natural Streams," Transactions of the American Society of Civil Engineers, Vol. 123, Paper No. 2934, 1958, pp. 641-684.